Structure and Life Cycle of Microburst Outflows Observed in Colorado

MARK R. HJELMFELT

National Center for Atmospheric Research, Boulder, Colorado*

(Manuscript received 21 May 1987, in final form 4 December 1987)

ABSTRACT

Intense, small-scale divergent outflows known as microbursts are held responsible for a number of aircraft accidents. This paper describes the morphology of microburst outflows observed in Colorado. Outflows are categorized into morphological types based on analysis of observations by Doppler radars and a surface meteorological network. Outflow life cycle is discussed, and the vertical and horizontal structure is described. Basic characteristics of microburst outflows are summarized from statistics compiled using both single and multiple Doppler analyses.

The microburst outflows are classified into two types: individual microbursts and microburst lines. Examples of observations of each type are shown. Organization of microbursts into microburst lines results in much longer-lasting wind shear than exists with isolated microbursts. The greater lifetime of microburst lines, combined with the much larger area of divergence, can create a much greater potential for hazard to aircraft than is the case for individual microbursts.

Outflow structure was found to resemble many features of the laboratory wall jet. Vertical profiles of horizontal velocity follow curves similar to those of the wall jet. Radial profiles of horizontal velocity through the microburst center also agree with the velocities predicted from wall jet theory out to the velocity maximum. Beyond the velocity maximum, microburst outflow velocities decay more rapidly than wall jet velocities.

Studies of microburst symmetry, as measured across the maximum velocity differential, reveal that the minimum shear is, on the average, only about 60% of the maximum. Implications of outflow structure and symmetry for aviation safety are discussed.

1. Introduction

Wind shear in the few hundred meters closest to the ground is held responsible for a number of aircraft accidents (Fujita and Caracena 1977; National Research Council 1983). Of particular concern is the intense, small-scale (0.4 to 4.0 km) divergent outflow known as a microburst. Outflows of this scale were inferred from observations during the Thunderstorm Program (Byers and Braham 1949) and were studied extensively in the Northern Illinois Meteorological Research on Downbursts (NIMROD) Program and during the Joint Airport Weather Studies (JAWS) Project (Fujita 1981; McCarthy et al. 1982).

The purpose of this paper is to describe the morphology of microburst outflows as observed in JAWS. Outflows are categorized into morphological types based on analysis of observations of outflows by Doppler radars. Outflow life cycle is discussed, and vertical and horizontal structure is described. Basic characteristics of each outflow type are summarized based on statistics compiled from single and multiple Doppler analyses. Many of the profiles and statistics were prepared in direct response to requests by scientists and engineers developing low-level wind shear detection and warning systems.

This paper is confined to a description of microburst outflow. Neither the origin of the downdraft air causing the outflow nor the dynamic forcing will be considered. These topics have been considered by Roberts and Wilson (1984, 1986), Knupp (1987), Srivastava (1985, 1987), Mahoney and Rodi (1987), Hjelmfelt (1987), and others, and is a major topic of current research at a number of institutions.

Microburst morphology has been discussed previously by Kessinger et al. (1983), Wilson et al. (1984), Hjelmfelt and Roberts (1985), and by Fujita in a number of papers and reports (especially Fujita 1979, 1985, 1986).

The most comprehensive descriptive discussion of microburst morphology was given in Fujita (1985). Many features of outflow and parent storm structure are shown in the pictures and diagrams of case studies, providing an excellent intuitive description of microburst structure. In this work, microbursts and macrobursts were delineated, and the horizontal vortex (rotor), often seen on the leading edge of microburst outflows, was described. Fujita (1985) also described

* NCAR is sponsored by the National Science Foundation.

Corresponding author address: Dr. Mark Hjelmfelt, NCAR/ATD, P.O. Box 3000, Boulder, CO 80307.

microbursts with nearly symmetric outflows and those appearing as intense divergence in a strong, directional flow. The latter was named a traveling microburst and ascribed to storm motion. Series of microbursts along a line were also described but not identified as an important morphological entity as discussed by Hjelmfelt and Roberts (1985).

A more quantitative description of microburst outflow structure was given by Wilson et al. (1984). Important features considered in their study included outflow growth times, average intensities and sizes, and the vertical structure of horizontal velocities. Outflow symmetry was considered with respect to its impact on single Doppler observation. The present study represents an extension of the Wilson et al. (1984) paper.

Fujita (1986) described a laboratory model which exhibits many features of microbursts in nature. In particular, the laboratory flow shows the development of horizontal vortex rings (rotors). These features have been described for microburst outflows by Waranauskas (1985), Fujita (1985, 1986), and Kessinger et al. (1988).

Numerical simulations of microburst outflows have been performed by Krueger and Wakimoto (1985) and Proctor (1985, 1988). Recently, Anderson (1988) has performed a series of numerical experiments with a three-dimensional numerical model. His work indicates that a single downdraft will tend to produce a circularly symmetric outflow even if the downdraft is elliptical rather than circular. This suggests that asymmetries may be caused primarily by external environmental factors, or by superposition of individual small-scale downdrafts.

Glauert (1956) defined the impinging wall jet as occurring when a jet of air strikes a surface at right angles and spreads out radially over it. He also described the form of the vertical profile of the horizontal velocity within the horizontal outflow. Bradshaw and Love (1959) described experiments with impinging wall jets and discussed the transition from the downward directed free jet to the horizontal wall jet. They found that most of the transition occurred within a little more than one radius of the free jet downdraft and was complete at a distance of two to three radii. Poreh and Cermak (1959) discussed the change in horizontal velocity as a function of distance outward from the free jet centerline. Poreh et al. (1967) more completely described horizontal and vertical profiles of the horizontal velocity.

These wall jet studies have been extended to examine the effects of an external stream (ambient wind) on the wall jet by Bradshaw and Gee (1960), Kacker and Whitelaw (1968), and others. Results indicate that, to a first order, the wall jet flow in an external stream can be approximated by the superposition of the external stream with wall jet flow in a quiescent environment (Sadeh and Mukherji 1974). In this paper we will discuss the similarities between the impinging wall jet and the microburst and the applicability of the wall jet profiles to the microburst.

2. Data collection and analysis

The present study is based on data collected during the JAWS Project, which was held in the Denver, Colorado, area in spring and summer 1982, and also during subsequent research projects held in the Denver area in summer 1984: Convection Initiation Project (Wilson and Schreiber 1986) and the Classify, Locate, and Avoid Wind Shear (CLAWS) Project (McCarthy and Wilson 1985). The primary observing systems used in these studies consisted of three Doppler radars operated by the National Center for Atmospheric Research (NCAR), one S-band radar (CP-2), and two C-band radars (CP-3 and CP-4). Surface weather data in JAWS were provided by the NCAR Portable Automated Mesonet (PAM) network (Brock and Govind 1977). The average spacing of the PAM network in JAWS was about 4 km. Figure 1 shows the location of the JAWS radars and the PAM stations. Radiosonde data are available from National Weather Service releases at Denver Stapleton International Airport. During JAWS, additional soundings were made at 1100 and 1400 MDT. (All times, unless noted otherwise, are in mountain daylight time.)

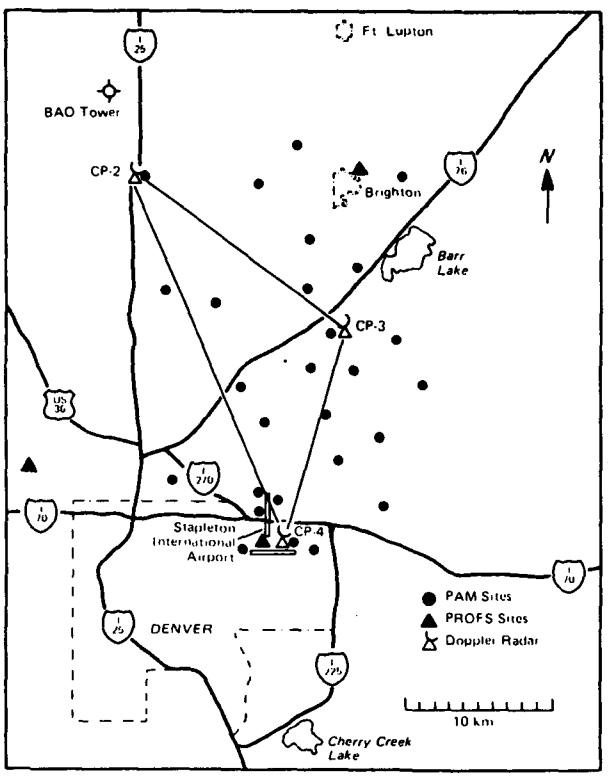

FIG. 1. Map of the JAWS Project study area. Surface networks and locations of Doppler radars are shown. Note location of CP-4 radar at Stapleton International Airport.

The JAWS radar network was specifically designed to collect high resolution radar and surface data to allow the structure of microburst outflows to be studied. Radar scanning was concentrated near the ground, with the lowest observed level centered 20–120 m above the ground. Scanning strategy permitted new volume scans to begin every 2–2.5 min. However, the small network and short lifetime of microbursts touching down at various places around the radars prevented full coverage of the entire lifetime of most microbursts by even one radar. Coordinated multiple Doppler data are available on fewer than 20 cases.

Wind fields were obtained from radial velocity data using an overdetermined dual-Doppler synthesis (ODDAN) program developed at the National Severe Storms Laboratory (Kessinger et al. 1987; Wilson et al. 1984) and the Custom Editing of Reduced Information in Cartesian Space (CEDRIC) program developed at NCAR (Mohr et al. 1986). Data editing to remove ground clutter contamination and range and velocity folding was performed on NCAR's Research Data Support System (RDSS), which is an imaging, interactive computer system (Oye and Carbone 1981). The vertical wind component was derived from an upward integration of the anelastic mass continuity equation. A zero vertical velocity lower boundary condition was assumed. Wind vectors were obtained on grids with 150 to 300 m horizontal and 200 to 500 m vertical spacing, near the maximum resolution available from the radars. This analysis scheme is the same as that used by Wilson et al. (1984). A more detailed discussion of the analysis techniques and estimation of errors is contained in that paper. Typically, analyzed wind features with scales greater than about 1.5 km should be well resolved, and some information is obtained for scales near 1 km.

Surface mesonet observations of microburst outflows in Colorado have been discussed in detail by Fujita (1985) and Bedard and LeFebvre (1986). Therefore, in the present study we will not discuss surface data, but rather concentrate on the higher resolution Doppler radar data.

3. Definitions

Analysis of JAWS data has revealed that microburst outflows can be categorized into two morphological types: individual microbursts (which may be simple isolated divergence features or embedded in strong, low-level flow) and microburst lines (Hjelmfelt and Roberts 1985; Hjelmfelt 1987). The following definitions are used in this paper:

1) *Individual microbursts.* Single microbursts with winds diverging outward in all directions from the microburst center, as in Fig. 2. The microburst may be defined in reference to Doppler radar observations of the diverging surface outflow such that the differential Doppler velocity across the divergence center must be >10 m s^{-1} and the initial distance between maximum

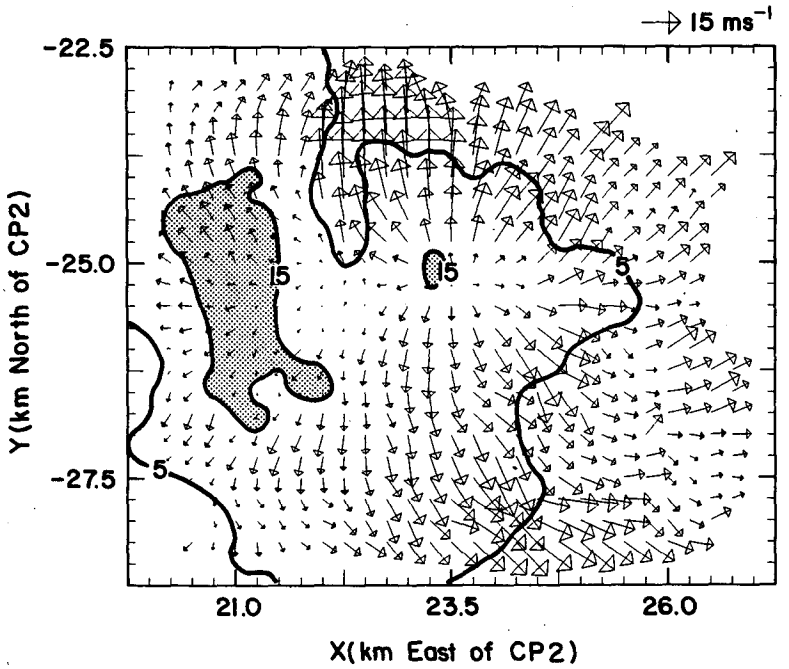

FIG. 2. Horizontal winds and reflectivity contours at lowest-level analysis (~50 m) for microburst A at 1445 MDT on 14 July 1982. Wind arrows are scaled as shown in upper right. Reflectivity contours in dBZ as shown.

approaching and receding centers must be <4 km (Wilson et al. 1984).

2) *Microburst lines.* A line of two or more microbursts, with outflows forming a continuous line of divergence outward from the line axis. The line is at least twice as long as it is wide (between velocity maxima on either side of the line). Microburst line structure is found to range from a series of nearly discrete microbursts along a line to a nearly homogeneous line of divergence, as in the example shown in Fig. 3.

Section 4 discusses microburst outflows. Examples of Doppler radar and visual observations are shown and outflow life cycle described. Outflow statistics of microbursts observed in JAWS and CLAWS are discussed and profiles of outflow structure are discussed in comparison with laboratory wall jet profiles. Microbursts which appear as intense divergences in strong directional flow are examined and operational implications discussed. Figure 2 illustrates that not all microbursts are symmetric. Many microbursts exhibit substantially stronger velocities, shear, and divergence along some radials than others. Outflow symmetry is considered in section 4b2.

Microburst lines are considered in section 5. Examples of microburst line outflow structure and radar observations are shown. Statistics of outflow size and life cycle are presented. Implications for detection systems are discussed.

4. Microburst outflows

Examples of microburst outflows are presented in this section. Photographs, single-Doppler radar observations, and multiple-Doppler wind fields are shown to illustrate the structure and life cycle of microburst outflows.

The photographs in Fig. 4, taken during the JAWS and CLAWS experiments, reveal many features of microburst outflows. Figure 4a, taken on 15 July 1982, shows a nearly circular complete ring of blowing dust, indicative of an isolated outflow. Blowing dust is often the only visual clue to a microburst from virga. Figure 4b shows a diverging rain shaft and evidence of a curl (horizontal vortex of rotor) at the leading edge of the outflow. This microburst occurred on 6 July 1984.

Figure 5 displays a time sequence of Doppler radar

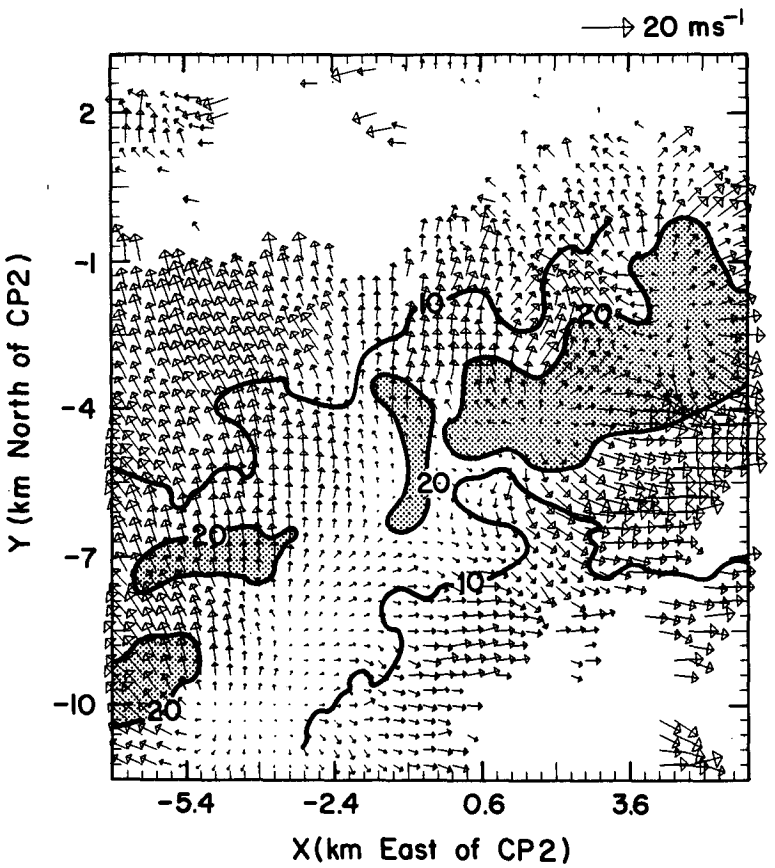

FIG. 3. Horizontal winds and reflectivity contours at 50 m for the microburst line at 1502 MDT 13 July 1982. Wind arrows are scaled as shown in upper right. Reflectivity contours in dBZ as shown.

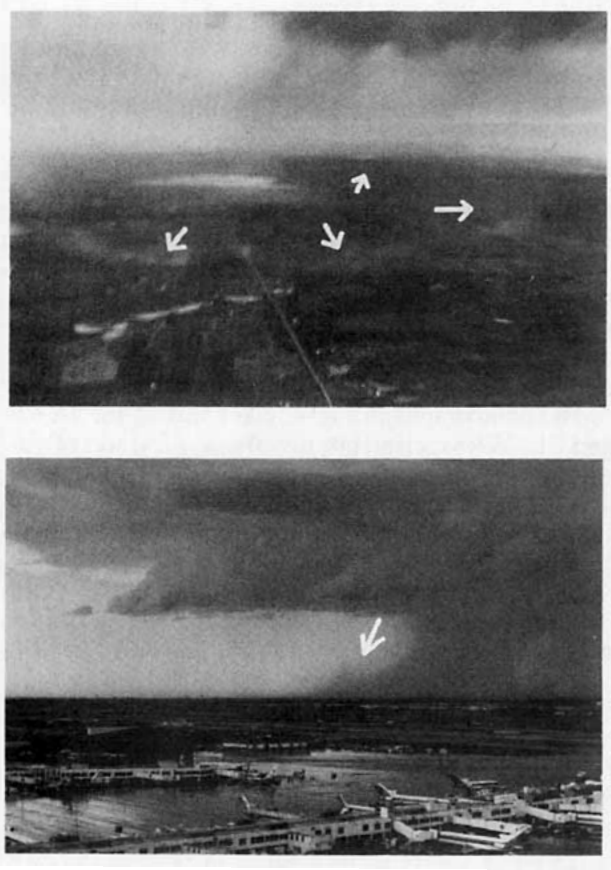

FIG. 4. Photographs of microburst outflows observed in the Denver area. (a) Photograph of dust ring observed at 1519 MDT 15 July 1982 from the Wyoming King Air (courtesy of Wayne Sand). Note that ring is continuous and nearly circular. (b) Photograph of outflow from heavy rainshaft at 1517 MDT 6 July 1984 taken from the Stapleton Airport Control Tower by Wendy Schreiber. Notice the curl at the leading edge of the outflow.

observations of a microburst on 14 July 1982 covering the period from 1638 to 1652 MDT. This case has been discussed previously by Wilson et al. (1984) and Fujita (1985). The sequence shows the gradual development and strengthening of the wind divergence in the first 8 min, and a subsequent decay of outflow strength over the following 6 min. Figure 5a shows the radial wind component as observed by CP-3 for five time periods. Figure 5b shows the corresponding lowest altitude horizontal wind field analyses, approximately 0.1 km. Figure 5c shows vertical cross sections through the microburst center along the line of storm motion. The grid for each time is translated according to the storm motion, 8 m s^{-1} toward 97° azimuth (az) (Roberts and Wilson 1984; Lee 1985, personal communication), but the wind fields show earth-relative flow.

At 1638 MDT, approaching flow is seen, but no receding flow; this is the first indication of an event. The analyzed wind field, Fig. 5b, indicates that there is no organized divergence at the surface. The vertical cross section reveals a downdraft aloft but with little evidence of divergence either at the surface or aloft. Some microbursts exhibit divergence aloft before the microburst reaches the surface (Fujita and Wakimoto 1983; Kropfli 1986), but this was not a common feature of JAWS microbursts (Wilson et al. 1984). By 1643 MDT, a clear divergence pattern has developed and a growing microburst is present. A well-defined, intensifying microburst is shown in the horizontal plot. The downdraft is also intensifying, as shown in the cross section plot, and a curl (horizontal vortex), *R*, is developing at the leading edge of the outflow. Peak velocity differential was observed by this radar at 1646 and reached 24 m s^{-1} over a distance of 4 km. The low-level wind plot indicates that the outflow is indeed at peak intensity at this time, exhibiting a well-developed isolated microburst divergent wind field. The microburst outflow is at its most symmetric form at this time, and the downdraft is at maximum strength. The weak horizontal vortex has now begun to move away from the core of the downdraft. At 1648, the microburst is just past peak intensity. The downdraft is also less intense than at 1646. The vortex is weak but well developed. At 1652, both the microburst downdraft and the outflow have weakened considerably. Peak velocity differential observed by the CP-3 is still near 20 m s^{-1} at this time, but as indicated by the horizontal wind plot, the microburst is decaying rapidly. The horizontal vortex is now much weaker and smaller. The outflow is also less organized and more asymmetric. The microburst dissipates over the next 4 min.

Horizontal vortices, as shown in Fig. 5, are common features of microburst outflows. They are not observed with all outflows, nor are they well defined in all directions for most microbursts in which they are observed. For example, at 1646, Fig. 5c shows a vortex on the upwind side, but none is evident on the downwind side.

a. Microburst characteristics

In this section, basic structural characteristics of microburst outflows are defined. Characteristic features of the growth and decay of microbursts are displayed, and parameters defining basic structural characteristics and life cycle for 27 outflows are tabulated. Representative life cycle and structural profiles are shown.[1] Analysis of microburst outflow structure has been guided, in part, by the needs and concerns expressed by scientists and managers developing operational detection and warning systems for microbursts; the figures and tables below represent a response to their questions.

1) CHARACTERISTICS OF MICROBURST OUTFLOW STRUCTURE AND LIFE CYCLE

Table 1 summarizes Doppler radar observations on the life cycle of microburst outflows from 26 JAWS

[1] Specific data requirements to produce a particular profile or statistic may severely limit the number of applicable cases.

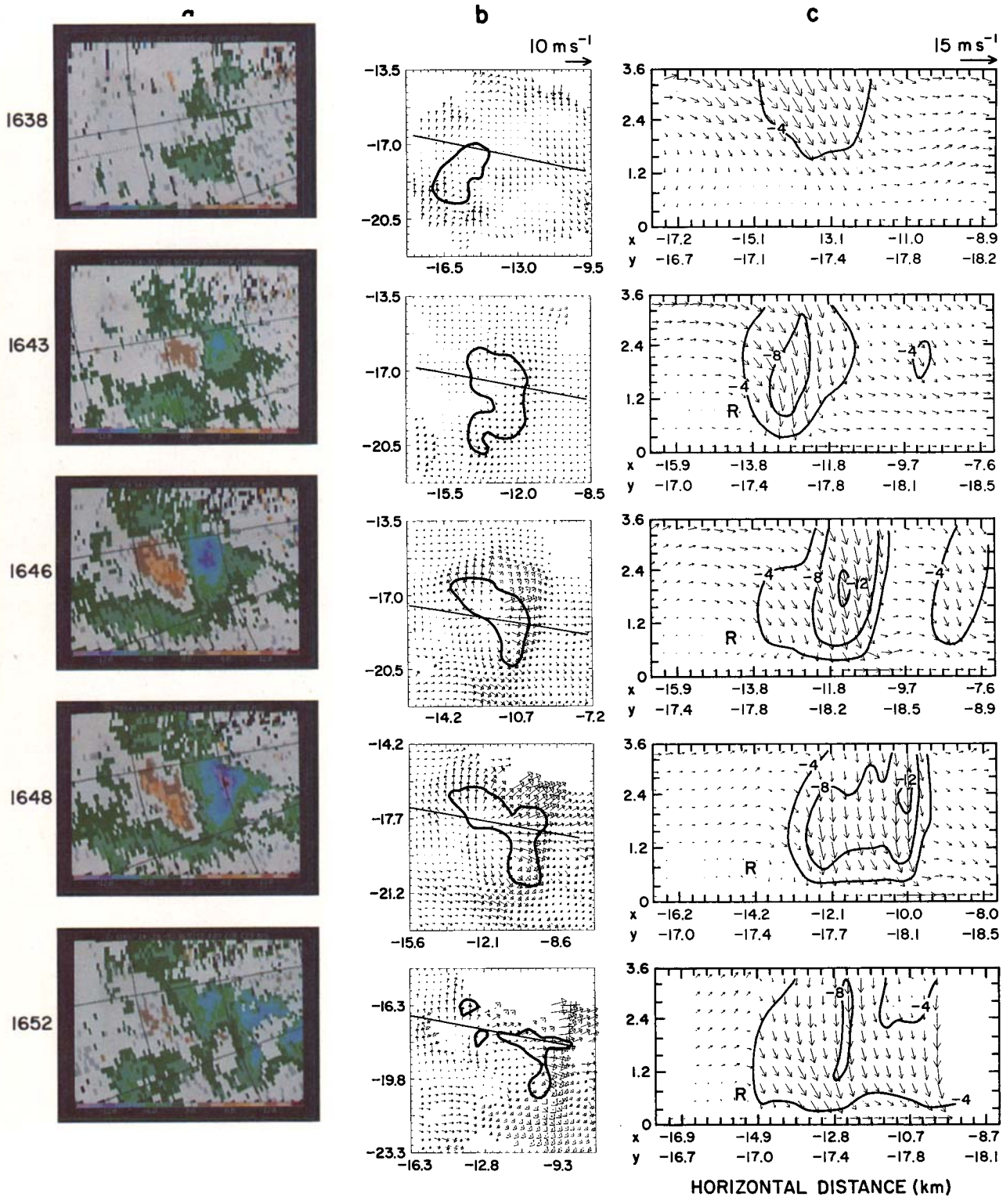

FIG. 5. Radar observations of the structure and life cycle of microbursts for 1638, 1643, 1648, and 1652 MDT 14 July 1982. (a) Doppler-velocity PPI display. The interval between colors is 2 m s^{-1}. Negative velocities are approaching the radar, positive velocities are receding. (b) Horizontal velocities and 40 dBZ reflectivity contour from 100 m AGL multiple-Doppler analysis. Black line indicates location of vertical cross section. (c) Vertical cross section of velocities in the plane and vertical velocities. Downdrafts contoured in 4 m s^{-1} intervals.

Table 1. Microburst Characteristics

Radar	Microburst	Location From CP-2 at MAX (°AZ/km)	Time Of MAX (MDT)	Initial		First Alarm		Max		Decay				Isolated or Embedded	Depth at MAX (km)	Reflectivity dBZ at MAX (dBZ)	Reflectivity dBZ at Vmax (dBZ)	Diameter (km)	Wmax at 1.2km ($m\ s^{-1}$)	Cloud Type	Cloud Base (kmAGL)	Mean Winds at Cloud Base (°As/$m\ s^{-1}$)	Surface Environmental Wind (°As/ms^{-1})
				Δt to MAX (min)	ΔV / D ($\frac{m s^{-1}}{km}$)	Δt to MAX (min)	ΔV / D ($\frac{m s^{-1}}{km}$)	ΔV / D ($\frac{m s^{-1}}{km}$)	E at MAX km	Δt to MAX (min)	ΔV / D ($\frac{m s^{-1}}{km}$)	Expansion after MAX	Decay Type										
CP3	23 May A_2	325/5	14:26	-5:00	14/1.6	-5:00	14/1.6	24/2.5	4.9	–	–	–	–	Isolated	0.8	55	30/50			isolated large cell	2.1	315/4kts	350/5
CP4	22 June 1	18/12	15:50	-16:00	4/1.0	–	–	18/3.0	4.3	+14:00		Yes	Weaken	Isolated	0.6	50	55/25			isolated cell	2.8	260/4	Light
CP3	22 June 2	50/14	16:09	-4:00	12/2.5	-4:00	12/2.5	14/2.5	4.8	+5:00	6/3	No	Weaken	Embedded	0.8	55	40/50			line of cells	2.8	"	190/5
CP3	22 June 3	155/7	16:14	-10:00	4/2.0	-3:31	15/2.0	18/2.5	6.0	+6:27	12/3	No	Large Scale	Embedded	1.1	50	50/33	1.2	6	along line of cells	2.8	"	170/7
CP3	22 June 4	113/12	16:16	-6:00	9/3.0	-4:19	12/2.0	12/2.0	3.2	+2:10	6/4	No	Large Scale	Embedded	0.4	40	10/40	1.6	9	along line of cells	2.8	"	210/11
CP4	22 June 5	10/11	16:23	-9:00	12/1.3	-9:00	12/1.3	16/2.3	5.0	+15:00	6/5	Yes	Weaken	Isolated	0.6	50		1.4	11	line of cells	2.8	"	Light
CP3	22 June 6	200/13	16:25	-10:00	4/1.0	-7:00	11/3.0	22/4.0	4.8	+15:00	9/6	Yes	Became part of line.	Embedded	0.9	55	30/45	1.4	9	line of cells	2.8	"	290/6
CP2	23 June A	90/18	16:53	-9:00	6/1.8	–	–	20/2.5	6.0	+7:00		Yes	Weaken	Isolated	0.9	55				isolated cells	2.1	326/4	
CP4	29 June G	76/36	16:05:59	-5:58	12/2.0	-5:58	12/2.0	24/4.0	6.5	+5:56	9/4	No	Weaken	Isolated	0.9	25	20/15	2.1	15	line of virga	3.5	290/5	Light
CP4	29 June C	75/33	15:51:15	-3:04	9/2.0	-1:16	27/3.0	27/3.0	5.0	+5:02	9/4	No	Weaken	Isolated	0.8	15	5/0			line of virga	3.5	"	Light
CP3	30 June A2	165/10	18:26:15	–	–	–	–	30/6.0	7.0	+9:20	21/14	Yes	Large Scale	Embedded	0.5	65	53/50	2.1	12	large scale	2.5	170/4	280/10
	8 July C	20/10	13:51:15	-14:59	6/1.0	-12:46	12/1.0	21/3.0	5.0	+16:23	9/8	Yes	Weaken	Isolated	0.9	30	20/20	1.4	0.8	line of virga	2.6	240/6	330/4
CP3	14 July A	150/18	14:45:15	–	–	–	–	42/5.0	5.6	+9.27	9/4	No	Weaken	Isolated	0.9	15	5/10			virga	2.8	280/8	Light
CP2	14 July C1	95/13	14:53:36	-5:16	12/3.0	-5:12	18/2.0	24/4.0	5.1	+5:08	18/7	Yes	Large Scale	Intermediate	0.6	45	45/34	2.2	12	isolated cell	2.8	"	355/7
CP2	14 July C2	105/30	15:13	-7:00	12/2.0			16/3.0		+8:00		No	Weaken	Intermediate	0.5	25	15/-			virga	2.8	"	345/5
CP3	14 July D	255/27	16:47	-7:00	12/2.0	-4:03	18/3.0	24/4.0	3.5	+6:00	9/3	No	Weaken	Isolated	0.3	50	25/20	3.1	13	isolated cell	2.8	"	280/8
CP4	20 July A_{12}	105/30	18:16:15	-7:15	9/1.0	-2:58	18/5.0	21/4.0	6.3	+5:00	12/3	No	Weaken	Isolated	1.1	25		1.8	14	weak isolated cell	4.1	350/4	360/3
CP4	5 Aug B1	281/15	18:31:15	-8:00	12/4.0	-8:00	12/4.0	27/7.0	9.0	+5:00		Yes	Large Scale	Embedded	0.4	55	40/40			large strong cell	2.2	350/6	170/5
CP4	5 Aug B2	300/18	18:29:43	-8:00	6/2.0	-6:00	12/2.0	24/4.0	3.6	+2:00	9/3	Yes	Large Scale	Embedded	0.9	60				large strong cell	2.2	"	170/5
CP4	5 Aug B3	275/13.5	18:48	-10:00	14/1.2	–	–	30/2.5	4.0	+13:00		No	Weaken	Isolated	0.5	55	45/45	2.0	22	large strong cell	2.2	"	170/4
CP4	5 Aug B4	265/10	18:48	-2:00	16/0.8	-2:00	16/0.8	18/2.0	2.7	+8:00	8/1	No	Weaken	Isolated	0.4	55				large strong cell	2.2	"	170/5
CP4	5 Aug C	270/7.5	18:34	–	–	–	–	26/3.0	5.0	+7:00	9/1	No	Weaken	Isolated	0.4	60				large strong cell	2.2	"	170/5
CP3	6 Aug A1	229/17	17:28:36	-8:34	6/2.0	-2:21	20/2.0	22/2.5	6.0	+3:09	18/4.5	Yes	Large Scale	Embedded	1.1	60	55/65			large strong cell	2.2	10/4	175/5
CP3	6 Aug A2	228/22	17:22:13	–	–	–	–	24/2.0	9.0			No		Embedded	0.6	50	40/45			large cell	2.2	"	150/5
CP4	6 Aug A_{24}	250/17	17:41:15	–	–	–	–	36/2.0	9.0	+9:10	9/1.0	No	Became line	Embedded	0.5	55	40/-			line of cells	2.2	"	160/6
CP2	6 Aug A5	193/34	17:52:44	–	–	–	–	30/20	8.5	+5:32	18/7.0	Yes	Large Scale	Embedded	1.2	60	25/33			strong cell	2.2	"	160/6
CP2	12 Aug A	225/23	14:34:20	–	–	-2.10	18/2.5	24/4.0	5.7	+5:25	27/7.0	Yes	Large Scale	Embedded	0.9	65	15/50			large strong cell	2.8	257/4	330/8
				-7:48	9/1.9	5:00	15/2.3	24/3.1	5.4	+8:13	12/4.5	12 yes/14 no	14W/9L 1 part of line	IS 13/12 EM	0.7	48	32/30	1.8	12		2.7		

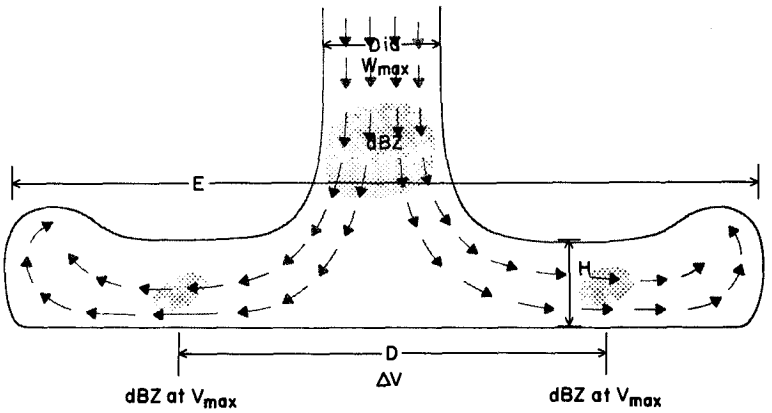

FIG. 6. Schematic of microburst characteristic parameters. (See Table 1.)

cases. Outflow structure parameters given in Table 1 are shown schematically in Fig. 6. Data include cases with maximum low-level reflectivity in the precipitation core ranging from 15 to >65 dBZ. Average maximum radial velocity differential, ΔV, at maximum intensity was 24 m s^{-1}, which occurred over a distance, D, of 3.1 km. Intensification from initial observed divergence to maximum radial velocity differential took a little more than 7.5 min. The outflow reached microburst intensity (first alarm) 5 min before maximum outflow intensity. On a few occasions, the microburst was already at microburst intensity when first observed. Average time between maximum intensity and decay was about 8 min, for an average total lifetime at microburst intensity of 13 min.[2]

At maximum outflow intensity, the distance between the outer edges of the outflow (outflow front), E, typically approached twice the distance between the velocity maxima, D. The distance E was found from high resolution single Doppler data by locating a region of convergence at the leading edge of the outflow.[3]

After reaching maximum intensity, about half of the microbursts continued to expand. Others weakened without further growth. Ultimately, some outflows grew beyond microburst scale and became larger-scale outflows before dissipating. A few outflows became incorporated into microburst lines.

In section 5b1, microbursts which appear as strongly diverging directional flow are discussed. In Table 1 these are labeled as embedded microbursts. Microbursts which appear as outflows radiating outward in all directions, as in Fig. 2, are listed as isolated. Roughly one-half of the cases were isolated microbursts and one-half were embedded. Embedded microbursts are associated with stronger surface-level ambient winds. Outflow depths, H, were often less than 1 km and averaged 0.7 km.

Reflectivities in the precipitation cores covered a wide range, 15 to 65 dBZ, and averaged 48 dBZ. Reflectivities at the velocity maxima were typically lower, averaging about 30 dBZ. Minimum reflectivity values

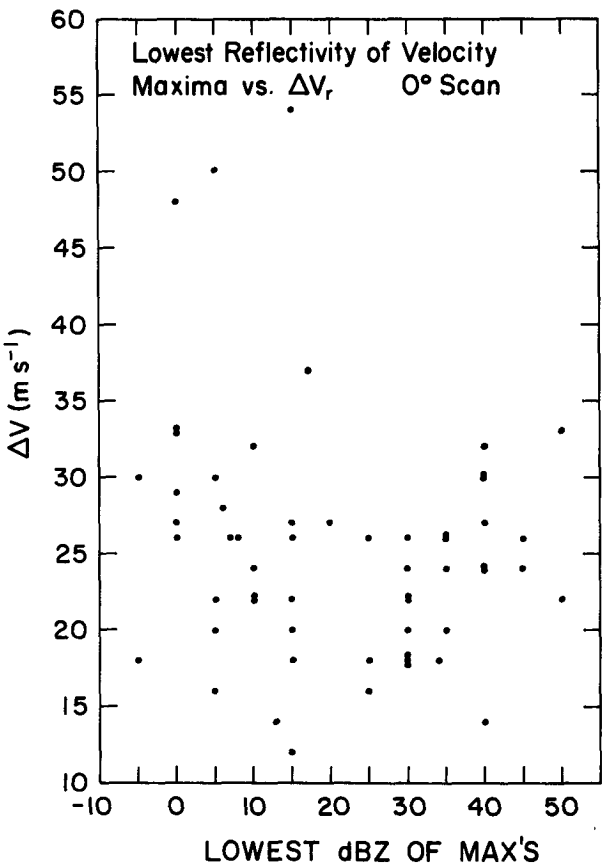

FIG. 7. Maximum radial velocity differential, ΔV, vs observed reflectivity in dBZ at the velocity maximum.

[2] The accuracy of these time estimates is limited by the radar scanning update rate of 2 to 2.5 min.

[3] This convergence is often only seen on one side, and is sometimes ambiguous. The values given in Table 1 are probably accurate to about ±50%. This estimate has been used in development of mathematical models of microbursts for use in detection algorithm development and for use in flight simulation.

at the velocity maxima approached 0 dBZ. This suggests that good radar sensitivity is required to observe microbursts in low-humidity environments. This point is illustrated in Fig. 7, based on nearly 50 cases. Reflectivity values at the velocity maxima are plotted against the observed velocity differential. It is apparent that some of the strongest microbursts (>25 m s^{-1}) occurred with very low reflectivities (<0 dBZ) at the velocity maxima.

Outflow morphology appears to be independent of precipitation rate. Maximum velocity differential has been found to be uncorrelated with reflectivity values in the JAWS dataset (Wilson et al. 1984). Also, one may compare the low-reflectivity microburst shown in Fig. 2 with the high-reflectivity 5 August 1982 case described by Elmore et al. (1986) as examples of similar microbursts with very different precipitation rates.

Downdraft diameters, based on 11 cases with analyzed wind fields, ranged from 1.5 to 3 km at 1.5 km AGL, with maximum downdrafts of 6 to 22 m s^{-1}.

Microbursts were produced by a variety of cloud types: isolated moderate-to-intense cells, lines of virga-producing cells, and short lines of intense cells. Cloud bases, estimated from soundings, were quite high for the low-reflectivity cases (3.3 km) and somewhat lower for the highest reflectivity cases (2.3 km).

2) Outflow profiles

Figure 8 shows two examples of the maximum radial velocity differential across a microburst, ΔV, as measured by Doppler radar and the distance over which it occurred, D, as a function of time and height to illustrate certain features of microburst outflows. These plots show that the microburst outflow rapidly achieves its full depth and, as the microburst dissipates, quickly decays in depth, maintaining a relatively constant depth during the microburst lifetime. Strengthening and weakening of velocity differential tends to occur simultaneously at all levels. The contours also reveal that the ΔV maxima are observed at low altitudes and that velocities decay slowly with height above. Figure 8a, for the 22 June microburst, suggests that microbursts may exhibit pulsating variations in intensity during their lifetime as seen by the secondary ΔV peak 5 min after the ΔV maximum. Pulsations may be indicated in the flight recorder data of Delta 191 which crashed at Dallas–Ft. Worth Airport in August 1985 (Fujita 1986), and are indicated in 6-sec interval Low-Level Wind Shear Alert System (LLWAS) data (W. Wilson and L. Cornman, personal communication).

The time–height profiles of D indicate considerable variability. The 5 August case (Fig. 8b) exhibits con-

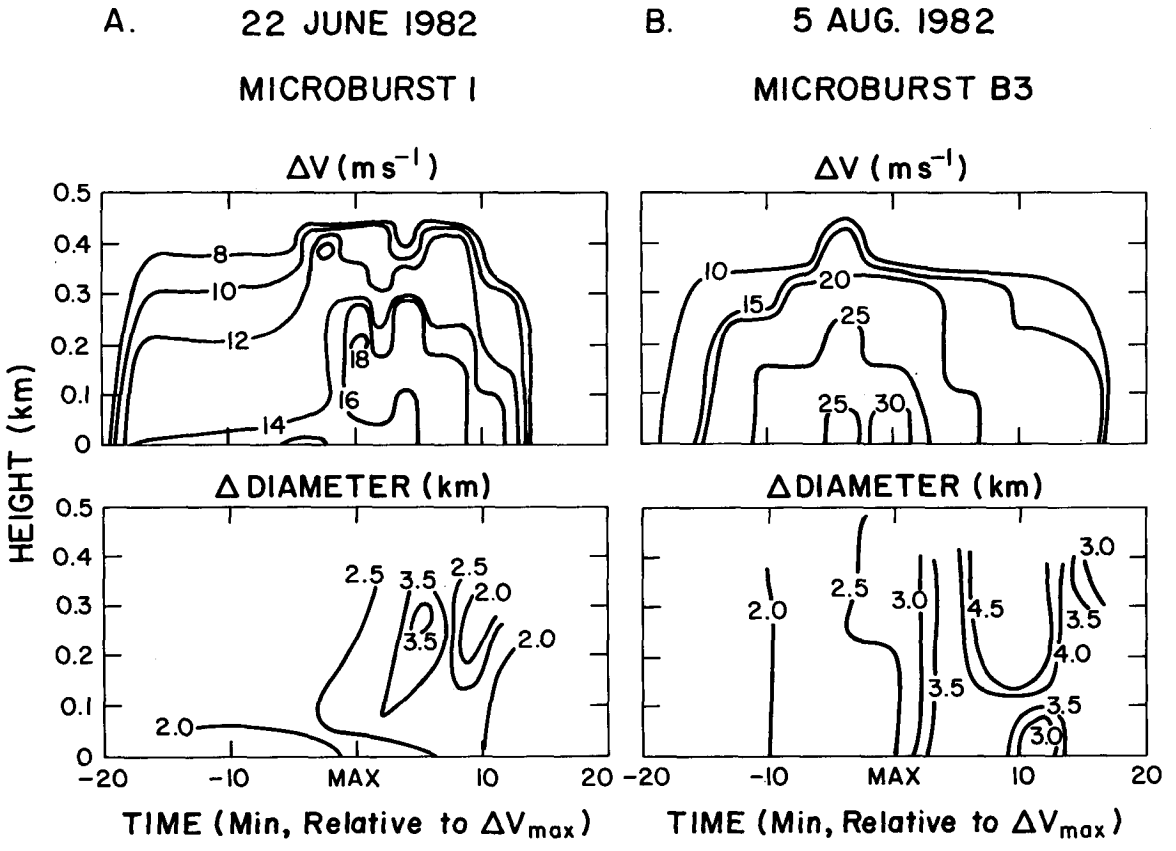

FIG. 8. Time–height profiles for ΔV and D (see text.) (a) 22 June microburst 1. (b) 5 August 1982 microburst B3.

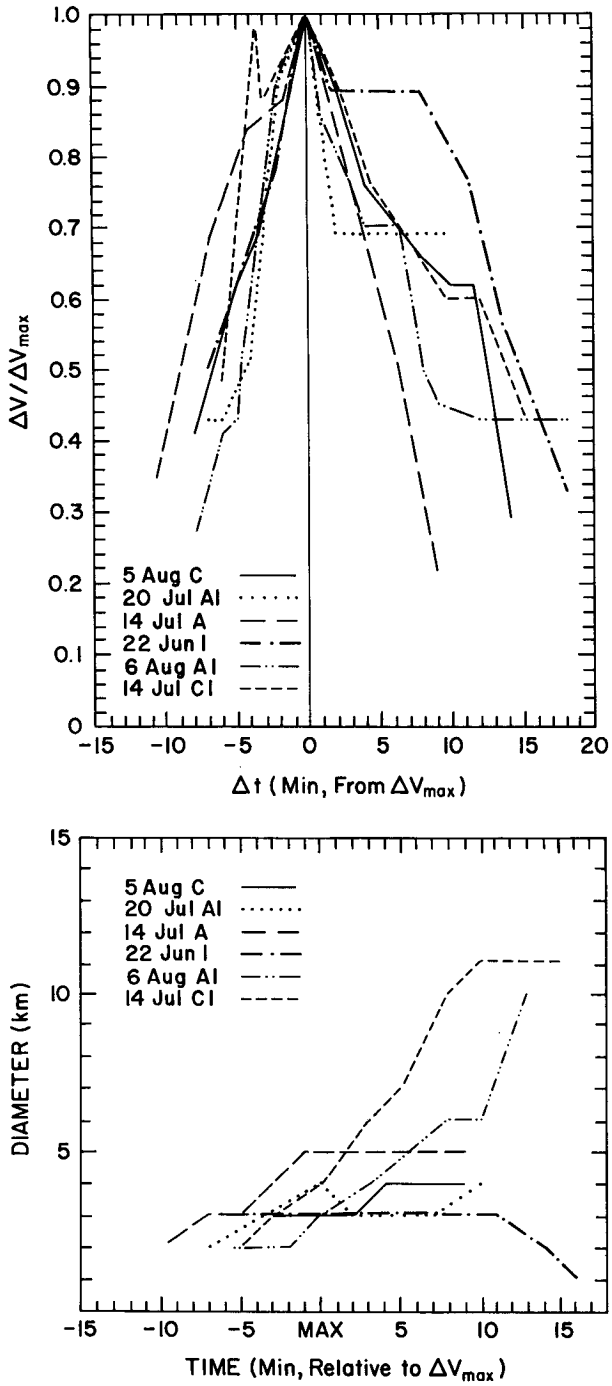

FIG. 9. ΔV and D as a function of time. (a) ΔV, normalize to maximum value for each microburst vs time. (b) Diameter, D, vs time for six cases. (See text.)

siderable growth with time, while the profile for 22 June does not. For both cases, relatively smaller values of D occur near the surface. Above the surface the pattern is less consistent with either height or time. Multiple-Doppler wind field analyses indicate that some variations are due to pulsations and fine-scale structure in the microbursts.

Figure 9 shows the changes in maximum ΔV and D as a function of time. In Fig. 9a, the radial velocity differentials are normalized to their maximum value, V_{max}, listed in Table 1. Figure 9a reveals that microbursts typically increase in strength nearly linearly from first observed divergence to maximum intensity. After a maximum value is reached, further pulses may occur; the microburst may exhibit a period of almost constant strength, or it may quickly decay. The distance over which this differential occurs, D, grows nearly linearly at first as the microburst strengthens to maximum intensity (Fig. 9b). After this initial growth, many microbursts exhibit nearly constant size until dissipation; others continue to expand, sometimes growing beyond microburst size (4 km across), and become larger-scale, less intense outflows.

Figure 10 shows ΔV and D at the time of maximum radial velocity differential as a function of height for eight cases and an average profile based on 12 cases. These profiles require very high quality data on microbursts located close to the radar. For these cases the microbursts were between 4 and 9 km from the radar. Elevation steps of 0.5°–1.0° provided for some independence between samples with data spacing of $\leq$100 m. Lowest angle scans may be biased to higher altitudes by blockage of the lower part of the beam (e.g., 0° $\approx$ 0.2°). As a similar figure in Wilson et al. (1984) shows, the maximum velocity differential is very near the ground, typically about 50 to 100 m, with velocities slowly decreasing in height above (Fig. 10a). Surface values of ΔV and D are smaller than those aloft primarily due to the retarding effects of friction.[4] The lower velocities near the ground are supported by surface mesonetwork observations (Kessinger et al. 1983). Aloft, D shows high variability, but an average over several cases at times near maximum intensity suggests that above the surface constant D with height may be a reasonable approximation, Fig. 10b. These profiles are similar to those obtained in numerical simulations of microburst outflows (Krueger et al. 1986; Proctor 1985).

Figure 11 shows a plot of normalized maximum radial velocity, V_{max}, as a function of normalized height for eight microbursts and an average profile based on 12 cases. V_{max} occurs at about 1.5 to 2.0 times the downdraft radius as estimated from multiple-Doppler analyses (Table 1). A wall-jet velocity profile adapted and rescaled from Poreh et al. (1967) is also shown. Wall-jet theory (Bradshaw and Love 1959) suggests that at the distance of V_{max}, the vertical profile of the horizontal winds should be approaching that of the well-developed wall jet. Comparison of the microburst out-

[4] Use of IF limiting techniques in the radar processor improves the ability of the NCAR radars to obtain reliable velocities near the ground. These techniques provide an ability to "capture" the stronger signal of either the clutter velocity or the meteorological velocity rather than a value biased between the two (Frush 1981; Nathanson 1969).

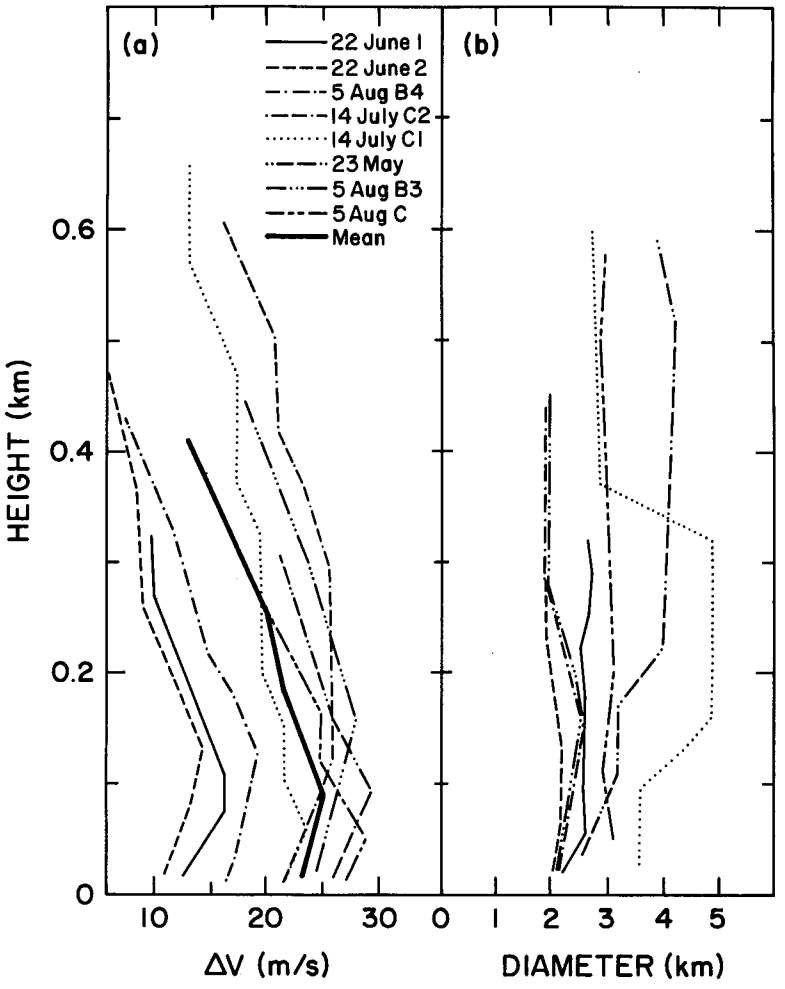

FIG. 10. Height profiles of (a) radial velocity at V_{max}. Solid line is average of 12 cases. (b) D.

flow profiles with the wall-jet profile shows considerable similarity.

Figure 12 shows the velocity of the outflow as a function of radial distance, R, outward from the center of the microburst at the elevation of the maximum measured velocity. Figure 12a shows velocity profiles six times during the life of (14 July 1982) microburst D (see Fig. 5). The curves indicate that near the time of maximum ΔV, the radial velocity profiles are relatively smooth and simple. As the microburst decays, the structure becomes more complicated. The 1650 and 1652 MDT curves show a bimodal structure with a secondary peak near 4.5 km from the microburst center. These secondary peaks are associated with the horizontal rotor that has advected away from the weakening downdraft (see Fig. 5).

Profiles of radial velocity as a function of distance from the microburst center can be scaled by V_{max} and the distance to V_{max}, R_{vmax}. Figure 12b shows several normalized curves for microbursts near maximum intensity and a curve for wall jets adapted from Poreh and Cermak (1959). Within the region of impaction under the downdraft and inside the velocity maximum, the velocity increase expected from wall-jet theory is proportional to r, the scaled radial distance from the center of the downdraft. A similar result would be expected from simple potential flow. The velocity maximum occurs beyond the region of impaction as the wall jet is setting up. Beyond the maximum, the decay in velocity expected for a wall jet is proportional to $1/r$. Figure 12b shows that within the impaction zone, the expected wall-jet profile is a reasonable approximation. Beyond the velocity maximum, the observed velocity profiles decay much more rapidly than those of the wall jet, at a rate proportional to $1/r^2$ or greater. One explanation for this discrepancy is that the wall-jet model assumes a steady state condition with the outflow edge far removed from the measurements. Simple radial expansion is the primary cause for velocity decay in the wall jet. For microbursts observed in JAWS, the peak velocity occurs at roughly half the distance to the edge. Developing horizontal rotor cir-

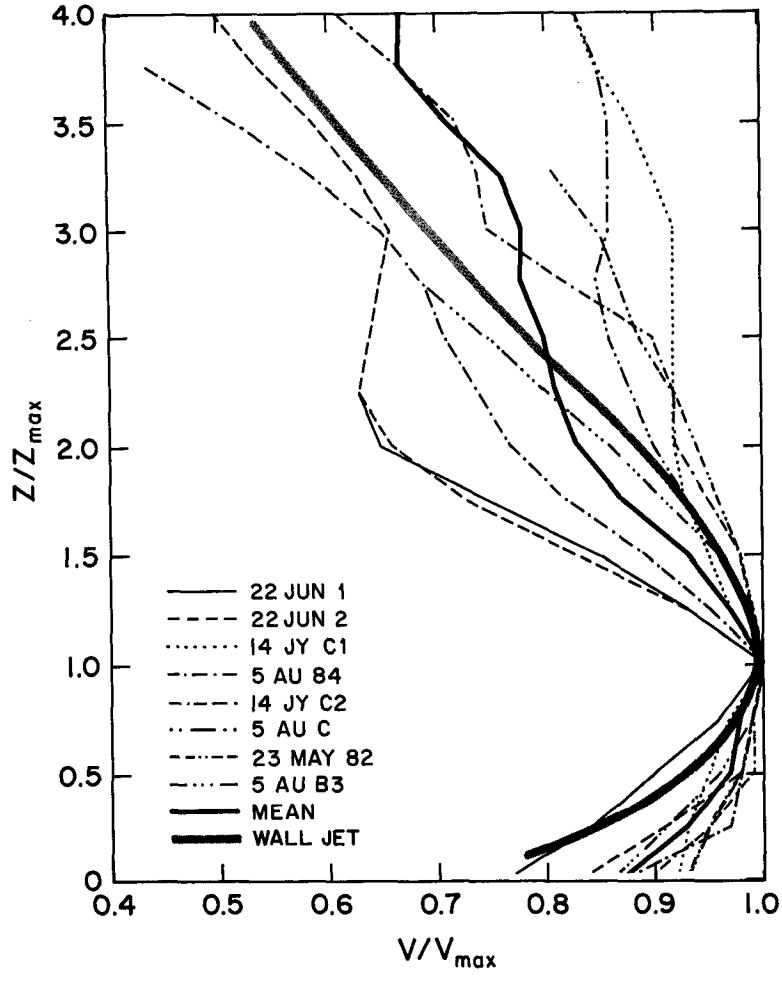

FIG. 11. Profile of normalized maximum radial velocity with height for eight microbursts. Velocity normalized on maximum value observed. Height scaled to height of velocity maximum. Heavy dark line is mean profile. Wide halftone line is profile expected for a wall jet (after Poreh et al. 1967).

culations are likely to be present, and much of the horizontal velocity is changed into the vertical. In some cases, the profiles are perturbed by outside environmental effects, e.g., obstacles, counteracting winds, etc. At distances increasingly farther out from the velocity maximum, these are more likely to become apparent.

b. Symmetry considerations

1) MICROBURSTS IN STRONG DIRECTIONAL FLOW

Figure 13 shows a strongly diverging directional flow. Such a flow pattern exhibits an apparent asymmetry and suggests that detection along the direction of flow may be difficult using radial velocities directly. This situation is similar to that described by Fujita (1985) who ascribed such a pattern to traveling microbursts (e.g., storm motion). This situation was not uncommon in JAWS (see Table 1) and has been a source of some concern in operational system development.

Figure 14 is a photograph of a microburst observed on 9 August 1982 during JAWS. The precipitation shaft is curved outward as it descends from cloud base to the surface. This is indicative of a substantial shear in horizontal wind below cloud base. As the precipitation falls into the sheared environment, the horizontal velocities of the particles adjust to that of the environmental flow; thus, the microburst flow field is perturbed by the low-altitude winds.

Figure 15 shows photographs of a color display of radar observations of a microburst observed on 22 June 1982 (Hjelmfelt 1987). Figure 15a shows observations from the CP-3 radar. This microburst, identified by arrows, appears as a simple isolated microburst from this viewing angle, 115° azimuth (az). Figures 15b, c, and d are taken from data collected by CP-4. From CP-4, 60° az, the flow is very much skewed toward receding velocities (Fig. 15b). If the mean low-level environmental flow of 11 m s^{-1} from 210° az is subtracted out, the approaching–receding wind pattern is seen

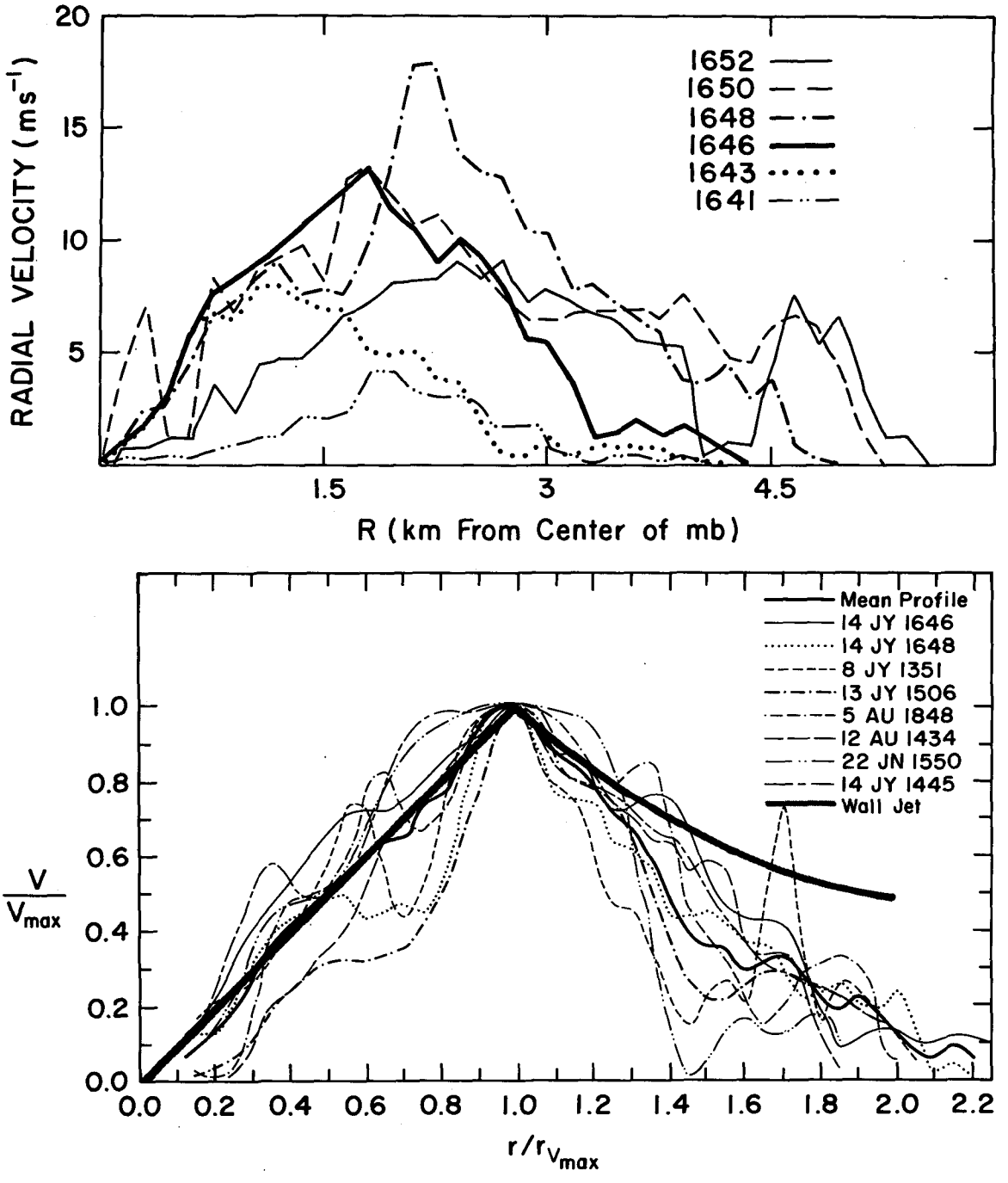

FIG. 12. Radial velocity along azimuth of V_{max} vs radius from microburst center. (a) Velocity vs radius for six times for microburst D on 14 July 1982 as observed by CP-3 (see Fig. 8.) (b) Normalized velocity vs scaled radius for several cases at the time of maximum observed ΔV. Velocity is normalized to the maximum for each microburst and radius is scaled to the radius of the maximum velocity. Heavy dark line is mean profile; halftone is profile predicted from laboratory wall jet studies.

(Fig. 15c). The diverging outflow of the microburst is also indicated by radial shear. Figure 15d shows a plot of radial shear averaged over 1 km distance.

The analyzed wind field for this microburst is shown in Fig. 16. In Figs. 16a and 16b, the low-level flow is plotted in absolute and eddy (mean wind removed) wind fields. Diffluence of the strong southerly flow is visible in Fig. 16a, but when the mean low-level flow is removed (Fig. 16b), the radially diverging pattern of the microburst is clearly seen. Vertical cross sections are shown in Figs. 16c and 16d. Figure 16c shows the cross-wind section. In this section, the downburst looks very much like an isolated microburst. Figure 16d shows the along-wind section. In this section the shear-

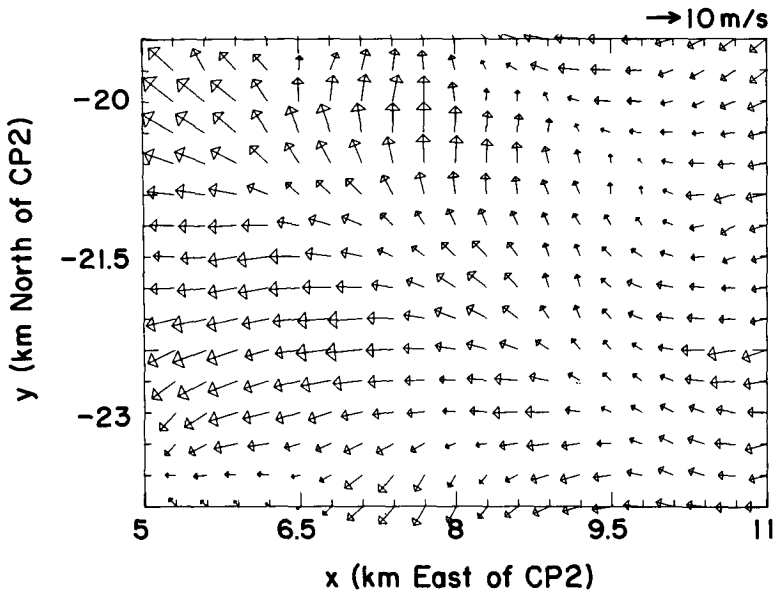

FIG. 13. Horizontal winds at 100 m for a microburst manifested as a strongly diverging directional flow. Wind arrows are scaled as shown in upper right.

ing of the downdraft downwind and the shift of the outflow in the direction of the low-level flow are seen.

The microburst shown previously in Fig. 5 occurred in weak surface flow and thus exhibited a simple isolated outflow pattern despite an 8 m s^{-1} storm motion. Conversely, the microburst in Figs. 15 (p. 913) and 16 was embedded in strong low-level flow, 11 m s^{-1}, and exhibited an embedded outflow pattern, though little storm motion was observed (Hjelmfelt 1987).

This suggests that storm motion determines the translation of the microburst, while the flow is perturbed by subcloud environmental shear. The result is somewhat analogous to that of cumulus turrets growing in a sheared environment. Further, the apparent asymmetry in the vector wind field is largely eliminated by removal of the low-level environmental wind, suggesting that this is not a cause of real outflow asymmetry. These results are also in agreement with results of the numerical microburst model studies of Anderson (1988) and the wall-jet studies of Sadeh and Mukherji (1974). Automated detection algorithms based upon radial shear, such as that of Merritt (1987), are not hampered by embedded microbursts. These observations suggest that there is no inherent physical morphological difference between isolated and embedded microbursts, but that embedded microbursts could be treated as the superposition of an isolated microburst and the environmental flow stream.

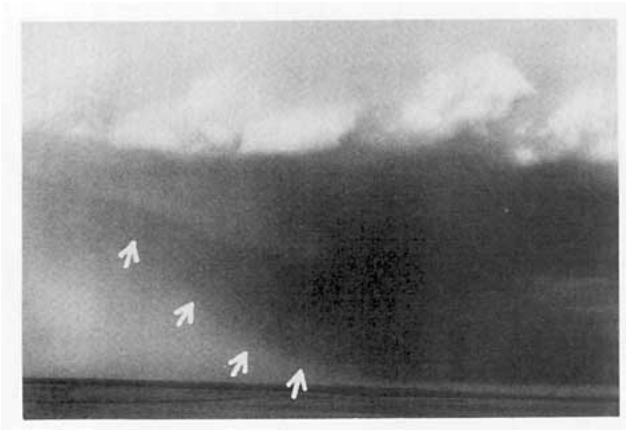

FIG. 14. Photograph of a microburst outflow embedded in a strong low-level ambient wind taken at 1719 MDT 9 August 1982 during JAWS. Note the curvature of the rain shaft. (Photo courtesy of Ed Szoke.)

2) MICROBURST OUTFLOW SYMMETRY

Wilson et al. (1984) examined microburst outflow symmetry in multiple-Doppler analyses of 13 microbursts by comparing shear values across the microburst center at 15° az increments over several fixed diameters. They found that, on the average, the minimum shear was less than half of that along the axis of maximum shear and that the asymmetry increased with increasing diameter.

For many applications an important parameter is the maximum velocity differential across the microburst, ΔV, which may occur over different distances, D, at different azimuthal angles. Eilts and Doviak (1987) suggested that shape of the reflectivity core might be a useful symmetry parameter. Another relevant parameter might be the shape of a divergence contour. These statistics are given in Table 2.

In this study, asymmetry of the wind field was determined from multiple-Doppler analyses for 14 cases in a manner similar to that of Wilson et al. (1984) and

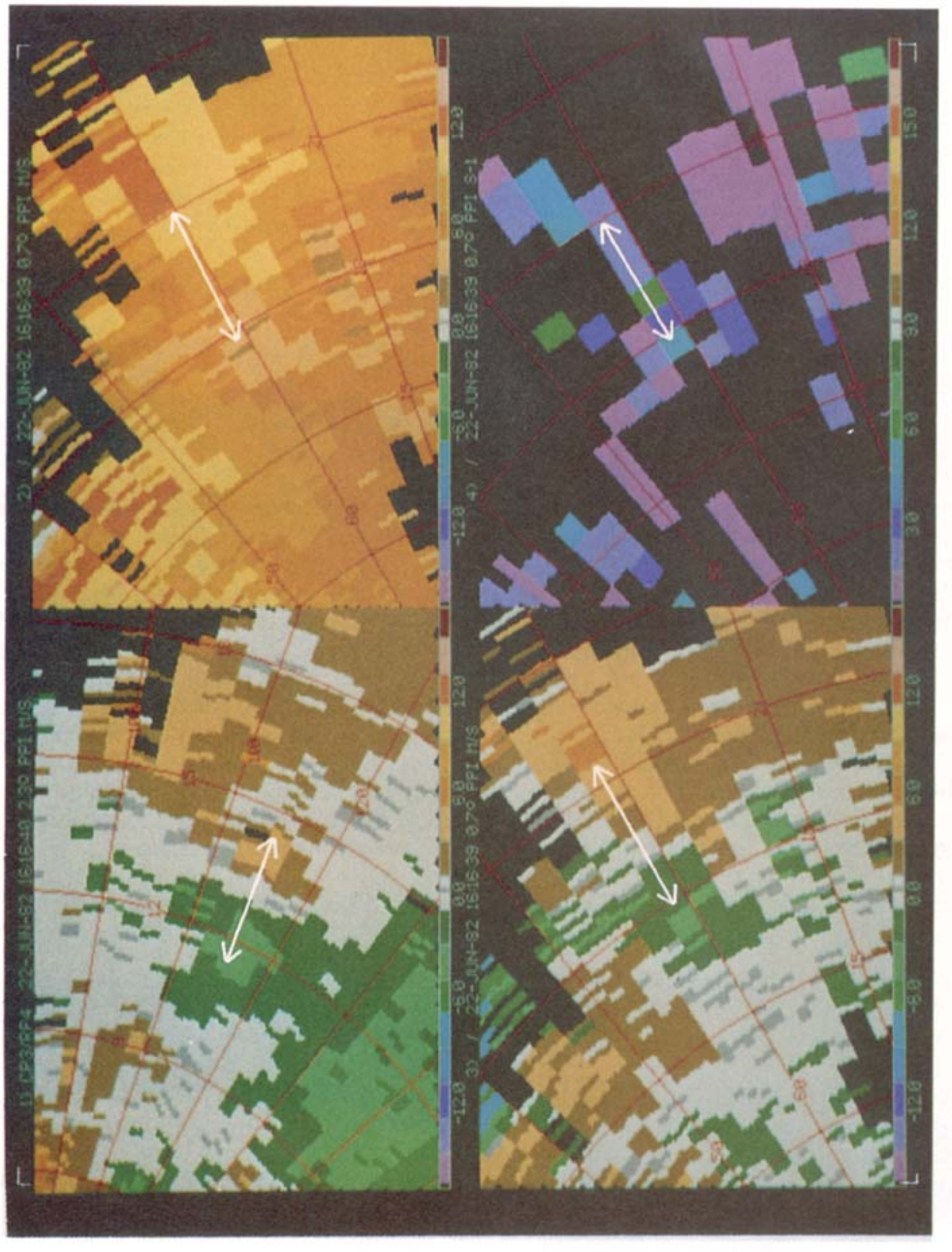

FIG. 15. Doppler velocity and shear PPI display of radar observations at 1614 MDT 22 June 1982 of embedded microburst 4. The interval between colors is 2 m s^{-1}. Negative velocities are approaching the radar, positive velocities are receding. (a) Radial velocities observed by CP-3. (b) Radial velocities observed by CP-4. (c) Radial velocities from CP-4 with low-level environmental wind removed. (d) Radial shear from CP-4 $\times 10^{-3}$ s^{-1}, colors at 1×10^{-3} s^{-1} intervals. Microburst location indicated by white arrows.

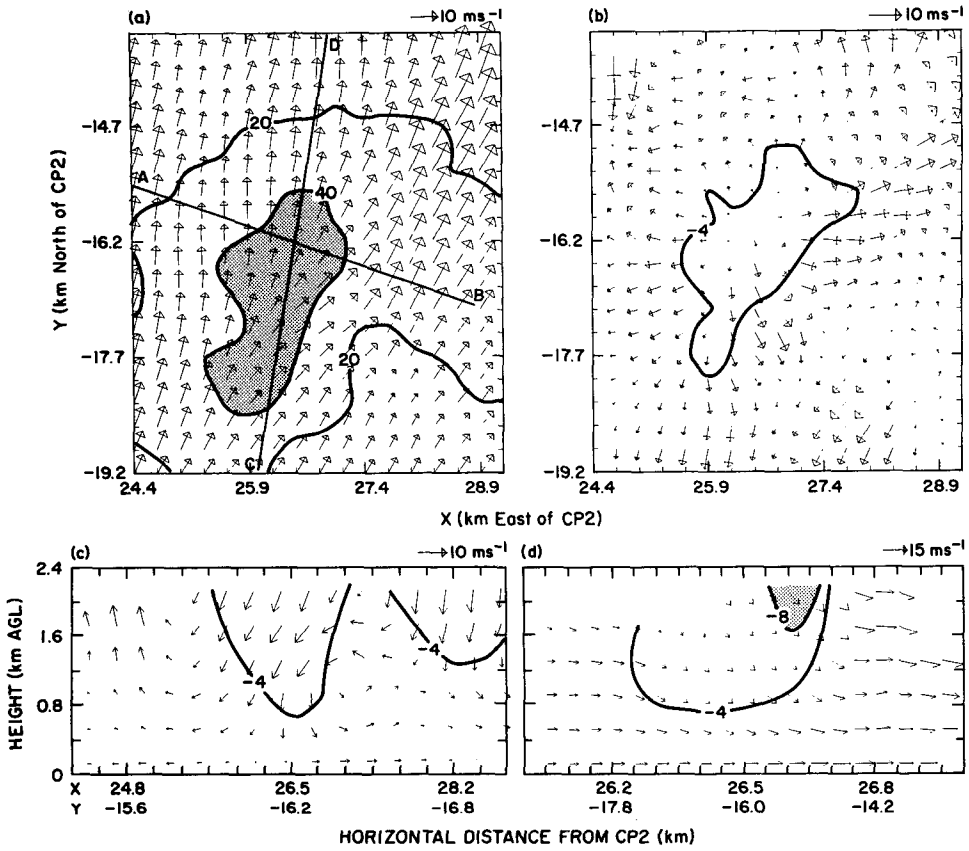

FIG. 16. Analyzed wind field for embedded microburst 4 at 1617 MDT 22 June 1984, derived from multiple-Doppler analysis, as in Fig. 3. (a) Horizontal winds and reflectivity in dBZ at 100 m AGL. (b) Eddy winds and divergence $\times 10^{-3}$ s^{-1}. (c) Vertical cross section of winds and vertical velocity (m s^{-1}) perpendicular to mean environmental flow. (d) Vertical cross section parallel to mean flow.

Eilts and Doviak (1987) (see Fig. 17). Vertical cross sections were plotted through the microburst center (divergence and vector center) at 15° az increments. The maximum velocity differential, ΔV, and the distance over which it occurred, D, were determined for each cross section. The maximum, ΔV_{max}, and minimum, ΔV_{min}, values were determined and ratios were taken. The azimuth of ΔV_{max} was found and the angle between ΔV_{max} and ΔV_{min} was calculated. Microburst line cases were excluded.

Divergence and reflectivity contours were obtained using the largest closed contour enclosed within the microburst outflow. Major and minor axes were determined and their ratio taken. Azimuths of the major axes were also found. Correlation of the values for each case with the ΔV ratio was also obtained.

Table 2 shows that the minimum ΔV is about half the maximum, and can be as small as one-third.[5] This means that a single-Doppler radar may see as little as one-third the maximum velocity differential. Converting the maximum and minimum ΔV values to shear, $\Delta V/D$, reveals that there is similar asymmetry in shear.

The orientation of ΔV_{max} does not show a consistent correlation with either cloud base winds or ambient surface-level winds. The angle between ΔV_{max} and ΔV_{min} averaged 75° with no values below 60°. With the arbitrary quantization of 15° used in this analysis, this result is consistent with an assumption that the angle between ΔV_{max} and ΔV_{min} is 90°.

The average ratio of the minor, L_{min}, to major, L_{max}, axis of the divergence contour is similar to that for differential velocity. However, the values for individual microbursts show little correlation with ΔV. In orientation, either the major or minor axis tended to be aligned with ΔV_{max}, but a consistent association was not found. Similar results were obtained for reflectivity. The choice of contour in many cases significantly affected the results.

Attempting to estimate symmetry from maximum ΔV values from two single-Doppler radars is difficult.

[5] Clutter contamination could potentially cause artificially-increased asymmetry and lead to erroneous angle estimates. It is not felt that this is true of the results presented here.

TABLE 2. Microburst symmetry.

	Horizontal winds (Multiple Doppler)						Single Doppler / Single Doppler	Divergence		Reflectivity	
Microburst	Time MDT	$\frac{(\Delta V)_{min}}{(\Delta V)_{max}}$	$\frac{D_{\Delta V min}}{D_{\Delta V max}}$	Shear $\frac{\Delta V/D}{\Delta V/D}$	Orientation az $(\Delta V)_{max}$	Angle $\Delta V_{max} - \Delta V_{min}$	$\frac{\Delta V_{min}}{\Delta V_{max}}$	Div. $\frac{L_{min}}{L_{max}}$	Orientation L_{max} (az)	dBZ $\frac{L_{min}}{L_{max}}$	Orientation L_{max} (az)
22 June (3)	1616	0.4	0.8	0.5	75	75	0.9	0.4	0	0.5	315
22 June (4)	1616	0.6	0.8	0.7	75	60	0.8	0.5	15	0.4	15
22 June (5)	1624	0.6	0.8	0.7	30	75	0.8	0.7	30	0.6	330
22 June (6)	1616	0.5	0.8	0.7	60	60	—	0.5	330	0.5	300
30 June	1827	0.4	0.6	0.6	315	75	0.7	0.5	350	—	—
8 July (C)	1352	0.6	0.9	0.6	0.0	90	—	0.5	75	0.5	60
14 July (A)	1445	0.5	0.6	0.8	0.0	90	0.6	0.5	75	0.5	330
14 July (C1)	1451	0.7	0.8	0.9	315	90	0.8	0.7	345	0.3	—
14 July (D)	1646	0.8	1.0	0.8	315	60	0.7	0.7	330	0.5	315
20 July	1819	0.4	0.8	0.5	60	60	—	0.6	60	0.4	345
5 Aug (B1)	1836	0.6	0.7	0.9	285	90	—	0.6	90	0.8	90
5 Aug (B2)	1836	0.4	0.9	0.4	90	75	—	0.5	300	0.5	60
5 Aug (B3)	1845	0.3	1.1	0.3	315	90	—	0.8	300	0.8	300
5 Aug (C)	1836	0.3	1.0	0.3	45	60	—	0.8	20	0.5	30
Mean	—	0.5	0.8	0.6	—	75	0.8	0.6	—	0.5	—
r	—	1.0	—	0.8	—	—	0.3	0.0	—	−0.2	—

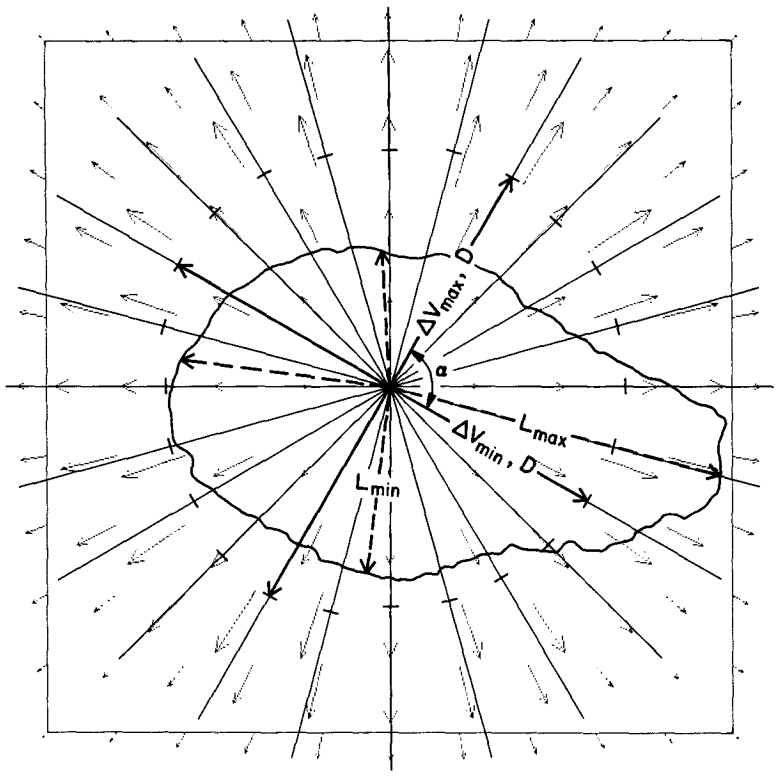

FIG. 17. Schematic diagram showing how symmetry parameters were determined.

Large acute between-beam angles are needed to ensure viewing of different velocity components. Random orientation of the microburst major and minor axes relative to the radar locations will lead to substantial systematic underestimation of asymmetry in most cases. An insufficient number of suitably scanned cases occurred in JAWS to overcome the above obstacles and provide reliable information by this technique.

c. *Summary of microburst outflow structure and life cycle*

The structure and life cycle of JAWS microbursts are summarized in schematic form in Fig. 18. Figure 18a shows the life cycle of the microburst. Initially, the descending downdraft and associated precipitation core (Roberts and Wilson 1984) have no observable wind shear ($T - 5$). Entrainment causes spreading and vorticity development at the leading edge of the downdraft, but no significant horizontally diverging outflow ($T - 2$). This feature is clearly seen in the laboratory model of Fujita (1986). As the leading edge of the downdraft reaches the surface, the microburst downdraft begins to spread in a manner similar to that expected from potential flow. At this point, the horizontal wind shear first becomes observable by Doppler radar. Typically, this occurs very near the surface (<500 m) and only a short time before surface-level divergence is seen (<1 min). Thus, Wilson et al. (1984) observed shear aloft before shear was observed at the surface in only 3 of 40 cases. As the downdraft reaches the surface, the microburst outflow begins to develop. The shear increases to microburst intensity (T) and begins to grow, becoming more organized as it does so. A stagnation zone directly under the downdraft core develops (Mueller and Hildebrand 1983). As the microburst reaches maximum intensity, the outflow is at its most organized, exhibiting many structural similarities to the wall jet ($T + 5$). The horizontal vortex (rotor) circulation develops and begins to move away from the downdraft core. Typically at the maximum, the return flow aloft in the rotor has not yet fully developed, but as the rotor moves away from the downdraft and the outflow starts to weaken, the full vortex becomes apparent ($T + 10$). The microburst may continue to grow, becoming a less intense (smaller shear and peak velocities), larger-scale outflow, or it may simply dissipate, becoming weaker and less organized over the next several minutes.

Figure 18b shows schematically the effects of vertical wind shear below cloud base on a microburst. The figure shows the case of precipitation falling into a region of strong surface winds. In the down-shear direction, curved precipitation streamers are often observed (see Fig. 14). In the cross-wind direction, the flow diverges in a manner similar to that of an isolated microburst. For moving storms in a strongly sheared troposphere,

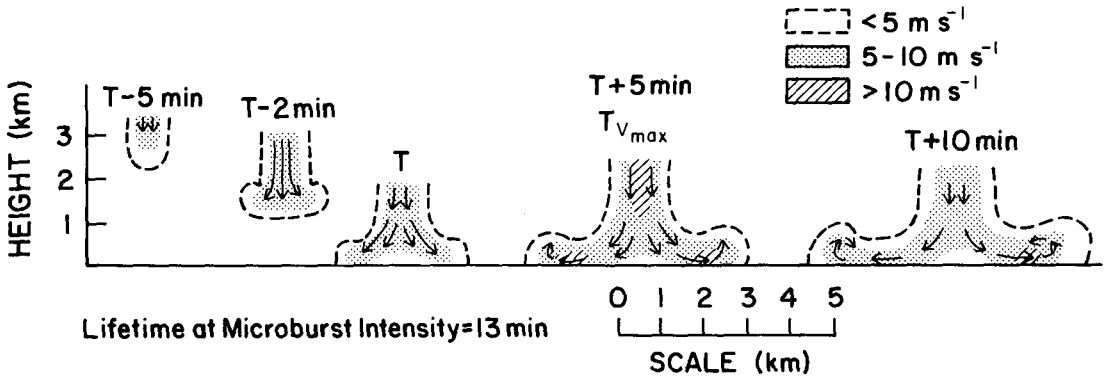

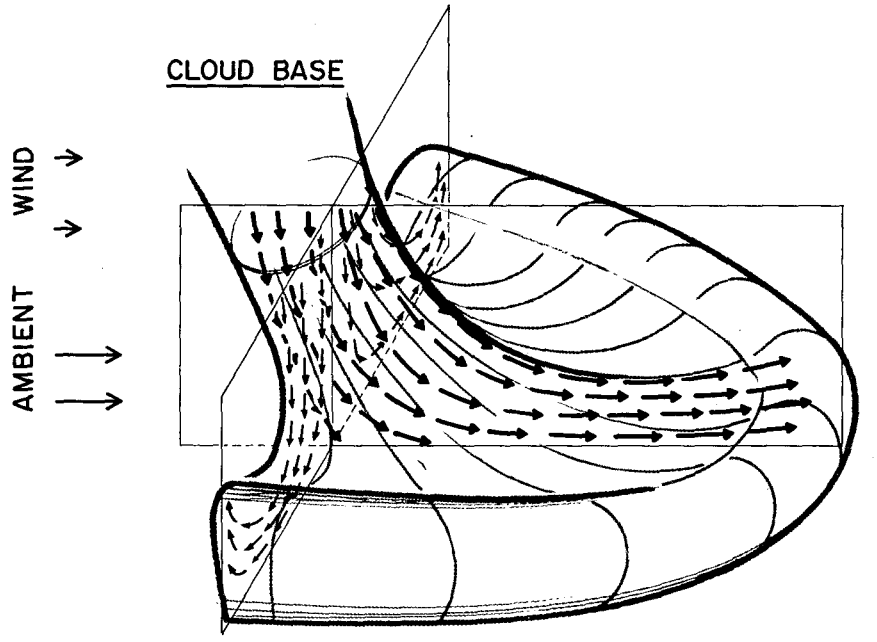

SCHEMATIC JAWS MICROBURST STRUCTURE
AT MAXIMUM INTENSITY

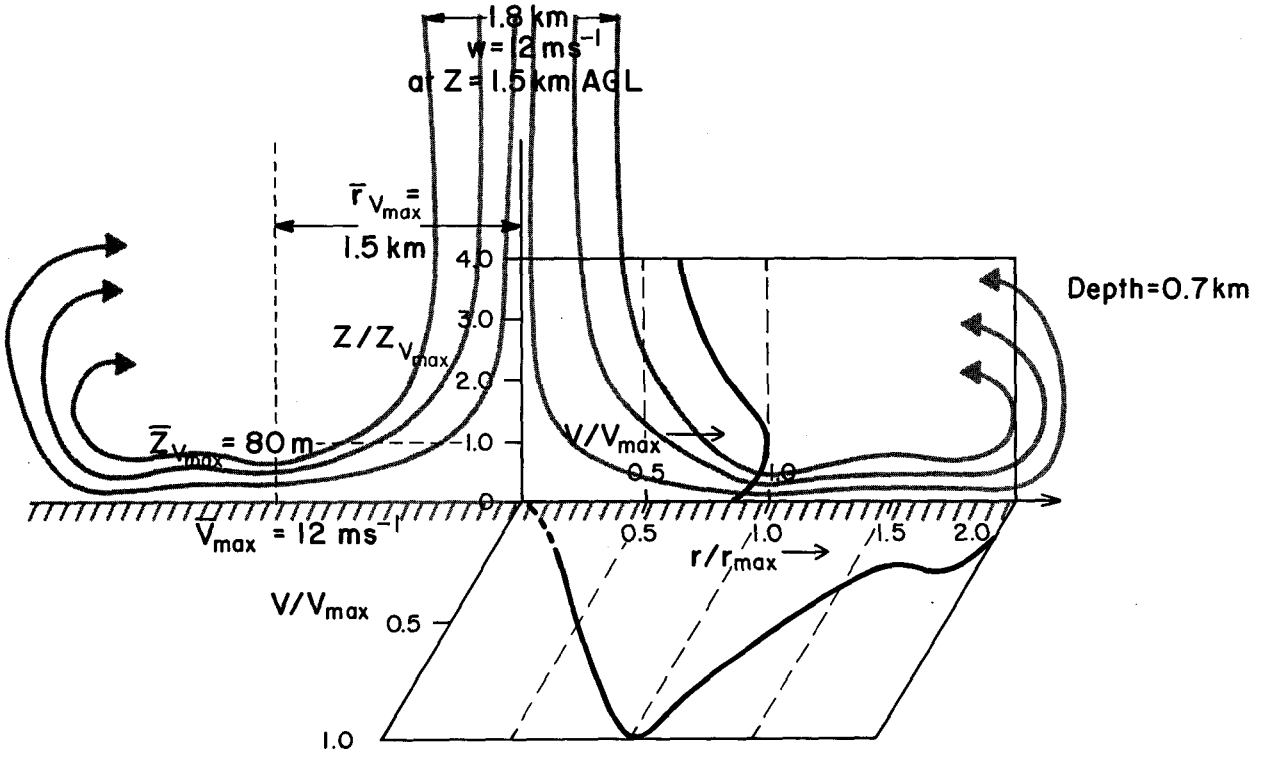

one might expect downward transport of horizontal momentum to be more important than was observed for the JAWS cases (Fujita and Wakimoto 1981). In these instances, a "bow" or "spearhead" reflectivity pattern might also be observed (Fujita and Byers 1977).

Figure 18c describes the structure of the outflow at maximum intensity. The schematic shows average values of several structural features. Velocity profiles based on Figs. 10–12 are also shown. As indicated in Figs. 12a and 18a, during growth phases the outflow field is becoming established and, at first, these profiles are not good representations. However, as the flow develops they become better approximations to the flow. During decay, the downdraft forcing is lost, the horizontal vortex moves off from the downdraft, and the structure becomes less defined. Results of simulations of microburst outflows are consistent with these profiles (Proctor 1988; Krueger 1986, personal communication). Similar profiles also have been found in microbursts observed in the Memphis, Tennessee, area (Rinehart et al. 1987).

5. Microburst lines

During JAWS it was observed that, on occasion, two or more microbursts could occur simultaneously, forming a line (Kessinger et al. 1983). Such lines often existed for an extended period of time through serial occurrence of microbursts at various points along the line.

Figure 19 shows a photograph taken from the Wyoming King Air research aircraft of a microburst line-producing storm (Hjelmfelt et al. 1986) during JAWS on 13 July 1982. Note the line of weak rain shafts descending from the cloud base. The microburst line is

FIG. 19. Photograph from the University of Wyoming King Air of the cloud line and rainshafts which produced the 13 July 1982 microburst line. Photograph taken at 1508 by Wayne Sand.

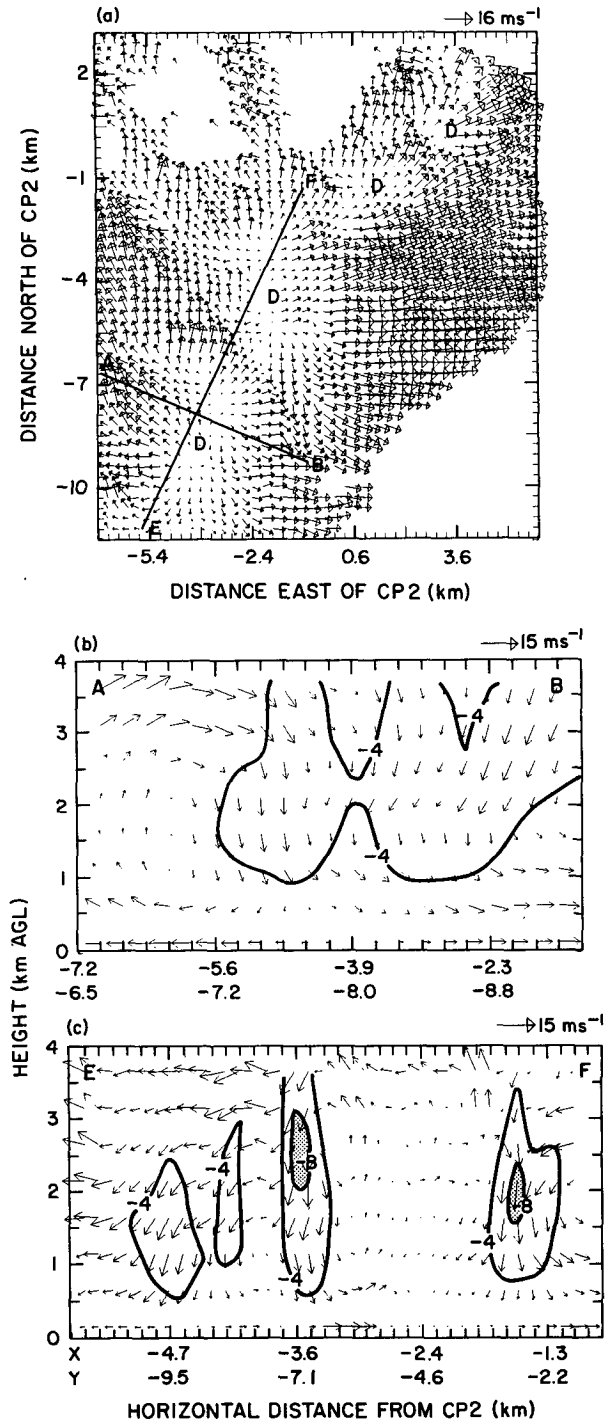

FIG. 20. Doppler radar derived wind field for the 1506 MDT 13 July 1982 microburst line. (a) Horizontal velocities at 50 m. Note the continuous divergence outward from line axis and divergence centers, *D*. Vertical cross section locations as indicated. (b) Vertical cross section of velocities in plane and contours of vertical velocity (m s^{-1}) perpendicular to the line axis. (c) Vertical cross section parallel to the line axis.

FIG. 18. Microburst schematic: (a) Life cycle, after Wilson et al. (1984). (b) Three-dimensional perspective of an embedded microburst. (c) Vertical cross section depiction of microburst structure.

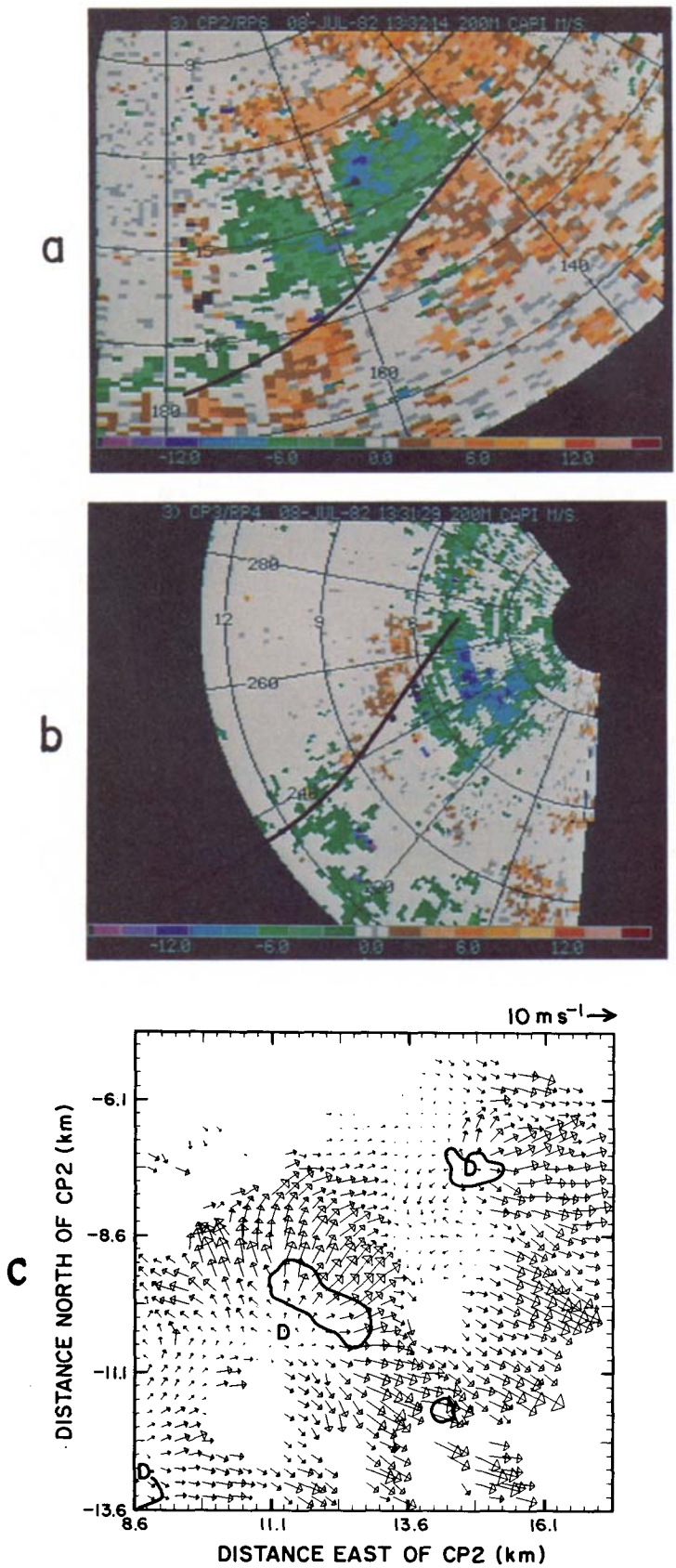

FIG. 21. Doppler radial velocities and multiple Doppler analysis for a microburst line on 8 July 1982. (a) Radial velocities from CP-2 at 1331 MDT shown for a 200 m constant altitude PPI (CAPPI) display. (b) Radial velocities from CP-3 at 1331 MDT for 200 m CAPPI. Analyzed divergence line location shown by solid line. (c) Analyzed horizontal velocities and reflectivity at 200 m at 1341 MDT. Note the discrete nature of the line but also that there is continuous divergence outward from the line axis.

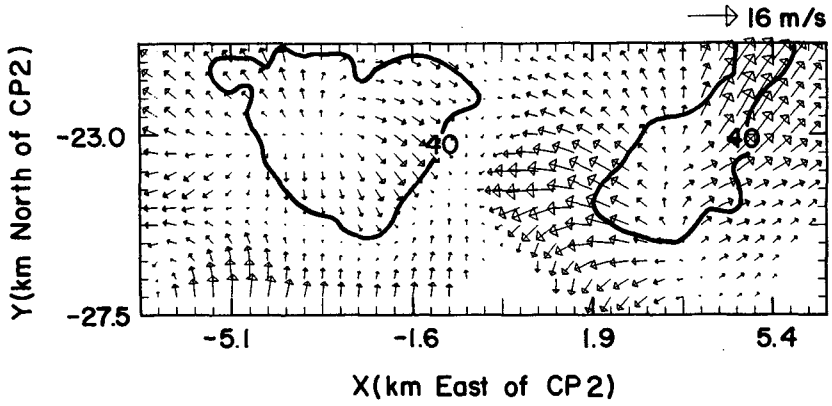

FIG. 22. Two nearby microbursts (B1 and C) at 1835 MDT 5 August 1982. Note that the microbursts are separate and that there is not a continuous divergence along the line between microbursts.

made up of the interacting outflows from these rain shafts.

The corresponding wind field from Doppler radar measurements is shown in Fig. 20. Figure 20a shows the low-level wind field at maximum divergence intensity. Notice that although the line is quite long, the divergence across the line is of microburst intensity with maximum divergence of $>7 \times 10^{-3}$ s^{-1}. Except for a more discrete microburst at the north end, the line appears rather homogeneous. This line might be approximated by a line of downdraft with outflow radiating outward on both sides and at the ends. However, closer inspection reveals that the line is actually composed of at least four interacting microbursts.

Vertical cross sections further illustrate the structure of the microburst line. In Fig. 20b, we see that for the transverse (cross-line) cross section, the microburst line exhibits the basic structure of the individual microburst, as in Fig. 5. In longitudinal (along-line) cross section (Fig. 20c), however, there is a series of downdrafts with an associated series of outflows. An airplane flying down the line at low levels would experience a series of alternating areas of downdraft and weak vertical motion or updraft and alternating headwind and tailwind components (Stevenson 1985).

Figure 21 shows radar observations of a microburst line which occurred on 8 July 1982. In Fig. 21a, the CP-2 radar views the line in a cross-line direction.[6] A line of divergence is seen, making it easy to identify this case. The CP-3, however, views the microburst line nearly down the line axis (Fig. 21b). Since most of the divergence occurs outward from the line axis, little divergence is seen; this case, which was quite clear from the other radar, might go unnoticed by CP-3. Multiple-Doppler analysis of this case (Fig. 21c) reveals that this line is made up of three discrete microbursts. This case can be contrasted with the more homogeneous outflow shown in Fig. 20.

Eilts and Doviak (1987) examined a microburst line which occurred in Oklahoma on 27 May 1984. Synthetic radial velocities derived from a multiple Doppler wind field for a fictitious radar located along the line axis indicated very little radial shear, but a long line of azimuthal shear. This result and the above observations suggest that microburst lines offer additional challenges for single-Doppler radar detection.

These examples show that microburst lines may exhibit nearly homogeneous divergence along their length or may be made up of a series of discrete microbursts. Most microbursts tend to be intermediate between the two, and may exhibit varying degrees of homogeneity during different stages of their life cycle.

If microbursts occur further apart, they appear as two nearby microbursts without continuous outflow along the axis. This is illustrated by the flow field from two nearly microbursts which occurred on 5 August 1982 (Fig. 22). The centers are about 6 km apart and the diverging portion of the outflows do not overlap. Typically in such cases, serial microburst production resulting in long outflow lifetime is not observed.

Microburst lines represent a higher order organization of downdraft production than individual microbursts. Lines do not represent a mere random close location of two or more microbursts, but a linear organization of downdraft production which may persist for a considerable period of time. Thus, we typically find much longer lifetimes for microburst lines than for their constituent microbursts or for individual microbursts. Organization of downdraft production has been shown for the 13 July 1982 case, for example. In this case, it was shown that convergence into the downdraft aloft occurred continuously along the length of the microburst line, not at isolated points (Hjelmfelt et al. 1986).

[6] To reduce ground clutter contamination, constant altitude displays at 200 m are shown.

Table 3. Microburst Lines

			Initial		MAX					Decay											
Case	Location at Max Relative to CP2 (AZ°/km)	Time of Max (MDT)	Δ t to Max (min)	Origin Type SM-sep mb's O-original	Δ V Max/Ave ($m\ s^{-1}$)	Length (km)	Width (D) at Max (km)	Width (E) Total (km)	Expansion	Δt to Max decay (min)	Decay Type W-weaken LS-large scale S-separates	Homogeneity H-homogenous D-discrete	Depth of outflow (km)	Reflectivity at Max (dBZ)	Reflectivity at Vmax + - (dBZ)	# of MB's Max Ave	Movement direction/vel. (AZ°/$m\ s^{-1}$)	Orientation of the Line (AZ°)	Mean Winds at Cloud base (AZ°/$m\ s^{-1}$	Cloud Type	Cloud Base (km)
22 June 82	CP2 110/21 180/21	16:39:52	-28:43	SM	27/12	21	3	6	None	+11:42	W	D	1.0	60	40,35	6,3	None	260	260/5kts	Lg. Cells	2.8
29 June 82	CP4 75/40 85/38	15:37:38		line present on first scan	22/10	10	2	4	In decay stage	+11:47	W	H	–	40	15,25	2,2	None	180	270/10	line of cells	3.3
29 June 82	CP4 70/28 85/26	15:51:15	-09:27	SM	26/12	10	2.5	8	None	+06:20	S	D	–	20	20,10	3,3	None	205	270/10	line of cells	3.3
29 June 82	CP4 75/35 80/36	15:50:39	-04:39	0	28/14	5	2	5	None	+06:56	S	D	2.0	30	15,5	2,2	None	350	270/10	line of cells	3.3
8 July 82	CP4 140/16 170/14	13:29:06	-12:47	0	50/12.5	8	4	6.5	None	+17:36	W	D	0.9	30	-5,0	3,2	None	240	240/10	Sm. cells mving down line	2.6
8 July 82	CP4 341/33 315/30	13:35:37	-53:51	–	21/15	16	6	14	Yes	–	–	H	1.2	30	30,0	5,4	60/6.6	240	240/10	Line of cells	2.6
13 July 82	CP4 345/25 310/24	15:06:19	-10:05	0	20/12.	30	3	8	None	+14:27	W	H,D	1.4	30	15,15	5.3	None	220	225/5	Line of virga	3.0
14 July 82	CP2 90/14 110/15	14:53:36	-07:34	0	26/14	9	2.5	8	Near decay stage	+1:45:51	W	H,D	0.9	50	38,35	3,2	110/1.3	200	300/15	Single cell	3.3
13 June 84	CP2 270/20 335/23	15:07:08	-35:42	SM	24/18	25	4		None	–	W	H	2.2	45	10,20	2,2	None	235	210/10	Line wk. cells	2.9
18 June 84	CP2 47/22 130/20	08:30:39	-20:05	0	54/21	25	4		None	–	LS	H	1.7	55	15,15	3,3	90/5.6	180	225/20	Single strong cell	–
26 June 84	CP4 180/15 280/25	08:58:36	-43:43	0	30/18	20	2.5	15	None	+32:05	W	H	1.0	25	5,20	2,2	130/1.5	270	260/30	Wk. sm. cells	3.1
6 July 84	CP2 125/32 145/30	14:29:41	-10:17	SM	24/18	25	4	10	None	+33:07	W	D	–	65	50,45	4,3	None	240	280/15	Single strong cell	3.2
6 July 84	CP2 125/45 145/45	15:02:48	-12:51	SM	18/15	20	3	8	None	+43:35	W	D	2.2	65	35,30	3,2	120/6.4	210	280/15	Strong cell	3.2
19 July 84	CP2 100/32 130/35	17:52:50	11:48	Line present on first scan	3 2/17	20	4	8	None	+29:29	S	D	0.9	30	12,10	4,2	120/3.2	10	0/40	Line of virga	4.0
24 July 84	CP2 70/20 150/15	15:54:14	-15:23	SM	30/16	25	4	15	None	+1:01:29	S	H	0.8	65	40,40	5,2	None	220	–	Strong cell	–
27 July 84	CP2 90/25 135/32	19:16:46	-51:12	SM	18/12	22	2.5	10	Yes	+38:25	W	D	2.5	65	–	3,3	270/2.5	170	100/5	Line	2.8
28 July 84	CP2 105/45 115/45	17:12:21	-15:20	0	22/14	10	4	8	None	+30:38	W	H	2.2	60	45,40	2,2	None	20	355/10	Single cell	3.1
28 July 84	CP2 100/32 120/30	17:42:59	-05:04	SM	24/16	10	3	8	None	+30:41	S,W	H	1.5	60	50,30	2,2	300/2.7	20	355/10	Line	2.8
30 July 84	CP2 100/32 130/30	17:45:12	-25:37	0	18/10	14	4	15	None	+15:21	W	D	0.5	65	35,30	2,3	None	10	350/15	Line	2.8
9 Aug 84	CP2 110/52 135/50	16:47:20	-33:12	SM	26/18	19	4	11	None	+40:54	S	H,D	1.7	65	35,40	2,2	None	20	–	Line	–
			-22:00	9SMB/80	26/15	17	3.4	9.3	16 None, 2 yes	+35:54	W=12 S=5 SW=1 LS=1	D=9 H=8 H,D=3	1.4	49	26,23	3.2, 2.5	12 None, 8 yes				3.1

In the cross-line direction, a microburst line can be treated as a microburst, and the microburst profiles shown in Figs. 10–12 apply. In the along-line direction, the flow represents a superposition of outflows, as shown by Fig. 20c, and the exact profile depends on microburst spacing and strengths.

a. *Characteristics of microburst line structure and life cycle*

Over 20 microburst line cases have been identified in the JAWS and CLAWS datasets. These have been analyzed using single-Doppler techniques to define general characteristics. Lines represent approximately one-eighth of the microburst cases observed during the two projects.

Most microburst lines were produced by lines of virga or lines of thunderstorms, including, for example, multicellular thunderstorms and squall lines. A few occurred from more isolated storms. The predominant producer was the high cloud-base line of cells strongly capped aloft (often below 6 km AGL). Microburst lines originated as divergence lines or as single microbursts that combined and developed into lines. Decay was usually through a general weakening of the outflow, although a few separated into single microbursts, and at least one developed into a larger-scale outflow. During their lifetime, most microburst lines moved very little, though the 19 July 1984 line traveled nearly 20 km during its 40 min lifetime. Maximum observed translation speed was 8 m s^{-1}.

Table 3 lists general characteristics of microburst lines obtained from the analysis of these cases. The maximum ΔV value represents the maximum radial velocity differential occurring at any point along the line; the average ΔV represents the average along the line at the time of maximum observed ΔV any place along the line. Most microburst line outflows have one well-defined outer edge with a gust front, and one ill-defined edge where the outflow gradually blends with the environmental flow.

The average maximum observed ΔV was 27 m s^{-1}, and the overall average ΔV along the line was 15 m s^{-1}. Long lines tended to have somewhat higher average ΔV's than short lines. The width, D, at the maximum was 3.4 km and the "edge-to-edge" distance, E, across the microburst lines averaged about 9 km. Typically, microburst lines exhibited little further expansion after growth to maximum ΔV. The average outflow depth was 1.4 km. The outflow depth is somewhat higher than that for single microbursts. This is probably related to the interaction of the microburst outflows in microburst lines as indicated in the modeling results of Anderson (1988).

Reflectivities in the downdraft core at the time of maximum ΔV ranged from 20 to 65 dBZ, with an average of 49 dBZ. At the outflow velocity maxima, reflectivities were lower, averaging only 25 dBZ. The microburst lines were made up of at least two to six identifiable microbursts occurring simultaneously along their length; in most cases these numbers represent a lower bound estimate. Lifetimes of microburst lines averaged 58 min with one case lasting for over 2 h. Individual constituent microbursts, however, had lifetimes similar to single microbursts. Thus, more than a dozen constituent microbursts typically occurred during the lifetime of a microburst line. For one case, it was estimated that more than 40 were involved.

Of the 20 line cases examined in detail, nine were discrete, eight were homogeneous, and three exhibited both characteristics during their lifetime. The homogeneous microburst lines tended to be a little longer than the discrete lines. Average lifetimes and maximum ΔV's were similar.

Microburst lines tended to be oriented with the cloud base winds, predominantly in a south–north to southwest–northeast direction. It appears that microburst lines come predominantly from storms organized into lines and thus are related to the two-dimensional forcing of convection.

If we compare the characteristics of the microburst lines to those of individual microbursts (Table 1), we find that the maximum ΔV of lines is somewhat greater than for individual microbursts, while the distance between velocity maxima is similar. The outflow depth and length are greater for the microburst lines. Individual microbursts have average lifetimes at microburst intensity of about 13 min, while the microburst lines averaged nearly 1 h. Low-altitude reflectivity values were similar.

b. *Summary of structure and life cycle of microburst lines*

Figure 23 shows the structure of microburst lines in schematic form. Microburst lines typically begin as a single microburst which is joined by others along a line or, sometimes, as a strengthening of divergence along a line and the development of microbursts. During its lifetime, a microburst line may appear very homogeneous or discrete microbursts may be apparent along it. New intensifications (new microbursts) will appear at various points along the line during its lifetime. In some cases, there appears to be a general weakening along the entire line as the microburst line decays, while in others a single microburst is left as the line organization breaks up.

Figure 23 also shows line outflow structure with average structural properties indicated. In the cross section perpendicular to the line axis, the microburst line structure is generally very similar to that of an individual microburst. In longitudinal cross section, the line is similar in structure to that given by the superposition of the separate interacting outflows, as in Fig.

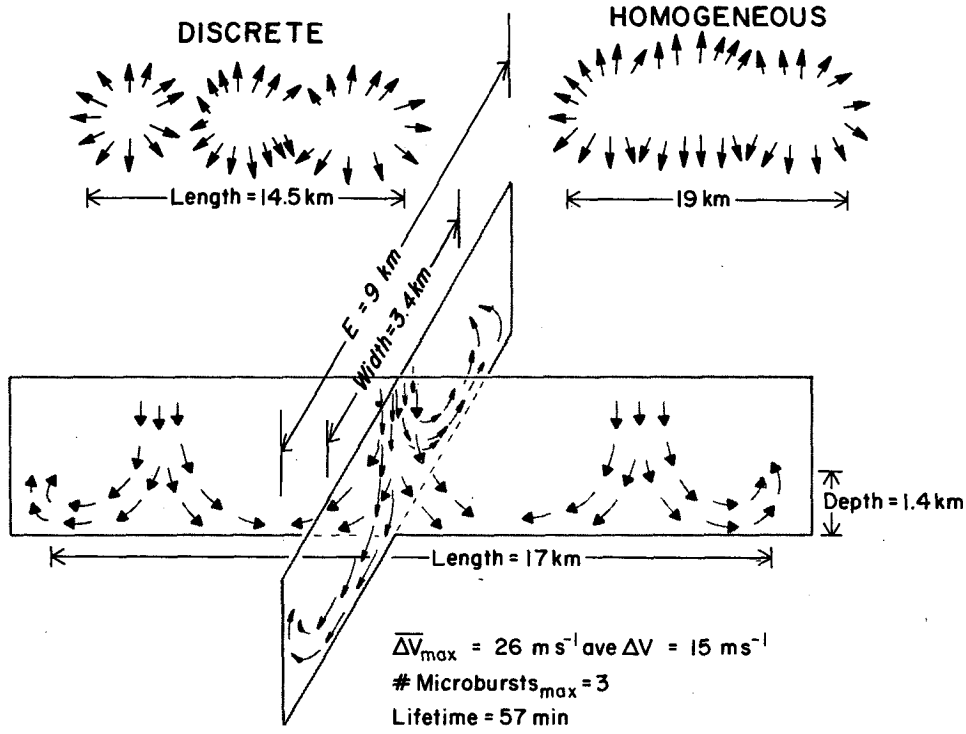

FIG. 23. Microburst line schematic: (a) Discrete and homogeneous outflows. (b) Perspective vertical cross section view of microburst line structure.

20c. This view is also suggested in the results of three-dimensional numerical simulations of two interacting microbursts (Anderson 1988).

6. Discussion

Aircraft safety considerations have prompted the adoption of a national wind shear plan (Federal Aviation Administration 1987). Components of the plan include modification of the Low-Level Wind Shear Alert System, development and deployment of a Terminal Doppler Weather Radar system, development of airborne instrumentation, and a major pilot training effort. Microburst outflow morphology has implications for all of these components.

Details of structure and life cycle of outflows and their variability can greatly affect aircraft performance during penetration (Elmore et al. 1986). Detection and warning strategies that are consistent with outflow structure must be developed. Pilot training, including flight simulation, must be based on realistic models of microburst outflows.

The structure of microburst outflows reveals that detection and warning systems must be able to account for the effects of environmental flow and microburst asymmetry. The results of this study and those of Wilson et al. (1984) suggest that these problems make the task of providing quantitative velocity component information along active flight paths much more difficult.

Based on the limited data from 14 cases, it was found that observed shear could be as little as one-third of that observed along a different angle. Given the finding of strong asymmetries in Oklahoma downbursts by Eilts and Doviak (1987), the asymmetry problem does not appear to be either an artifact of the JAWS data or restricted to the high cloud-based Colorado storms. It is suggested that reliable quantitative estimates of shear along a path at an appreciable angle to that observed by a single-Doppler radar may require combining radar data with mathematical modeling of outflow structure and mesonet data or even data from a second radar.

Microbursts appearing as a strongly diverging directional flow were explained as microbursts embedded in strong low-level winds. These microbursts may be difficult to observe in the radial velocity field; however, such microbursts are detectable using radial shear (Merritt 1987).

Normalized profiles of velocity with height and distance outward from the microburst center, as presented here, provide directions for the development of mathematical models to describe the three-dimensional outflow wind field. Such models are important for input to flight simulation, aircraft performance studies, and

detection and warning system development. Primary complicating factors are the presence of horizontal rotors and asymmetry.

Rotors are a significant feature in microburst structure. Fujita (1986) has indicated that they may play an important role in the microburst hazard to aircraft. Further study and analysis of rotor hazard to aircraft is needed. In some outflows, rotors have not been observed. In others, they only appear over a segment of the outflow circumference. Sometimes a complete vortex circulation does not develop until the time of maximum outflow intensity. The dynamics of microburst rotors also needs further investigation.

Fujita's (1986) analysis showing multiple rotor development and other evidence suggesting pulsating behavior in some microbursts deserves further attention. While pulsations may not be so severe as to interfere with microburst detection, they may have a serious impact on quantitative runway component estimation.

The analysis of Stevenson (1985) indicates the importance of the microburst line as an aircraft hazard requiring special attention. The microburst line may be thought of as the superposition of two or more microbursts and maintained by serial production of microbursts. The much longer lifetime and greater spatial scale of the microburst line lead to a much greater potential operational impact than for individual microbursts. This was illustrated in Stevenson (1985) and Hjelmfelt and Roberts (1985) by an example from the CLAWS experiment.

Table 4 lists pilot reports received by the Stapleton Air Traffic Control Tower as a microburst line crossed the airport on 19 July 1984, and summarizes the impact on flight operations. The pilot reports illustrate the severity of the effects of this line on arriving and departing aircraft and the changing effects as the line crossed the airport. The pilot who reported at 0000 UTC probably flew nearly down the axis of the line a few minutes earlier. The summary indicates a major operational impact over much of this period, including cessation of arrivals for 14 min and departures for 24 min. Ultimately, delays caused by the microburst line exceeded 45 min.

Microburst detection and warning must take into account microburst lines. For example, we note from Fig. 21 that a radar looking directly down the axis of a line might see very little radial shear. Not only does the elongated shape influence detection strategies, but the much greater lifetime may indicate a different response by aircraft and controllers.

TABLE 4. Impact of microburst line on aircraft at Stapleton International Airport.

Pilot Reports		
Time UTC	Runway	Pilot report
2338	(35L DEP)†	"lost 15 kts on take off roll"
2343	(35L DEP)	"moderate chop at 500 ft also"
2344	(35L DEP)	"at center field we had stagnation for 500 to 700 ft before airspeed increased
2351	(26L ARR)††	"+20 at 200 ft"
2353	(26L ARR)	"+20 at 500 ft and −20 to 25 inside 100 ft"
2355	(26R ARR)	"hit a real good sinker at 300 ft"
2357	(35L ARR)	"winds totally unusable"
0000	(35R ARR)	"better than an amusement park ride"
0012	(35L DEP)	"some shear at 400 ft"
0021	(8R ARR)	"a little wind shear about 100 ft out"
0022	(35L DEP)	"no wind shear"

Impact on Operations	
Missed approaches	12
Stopped approaches	14 min
Shift in arrival runway	2
Delayed departures	17 min, and 7 min
Shift in departure runway	1

† Runway heading 350° (north) on left side, departing aircraft.
†† Runway heading 260° (west) on left side, arriving aircraft.

7. Conclusions

This paper has presented a discussion of the structure and life cycle of microburst outflows. Individual microbursts were found to occur as isolated microbursts exhibiting radially diverging outflows and as embedded microbursts with outflows occurring in strong unidirectional flow. The radially divergent flow of the outflow is revealed when the mean low-level winds are removed. Microbursts can be organized into lines. Microburst lines represent a distinct morphological feature with important distinguishing characteristics of greater size and longevity.

Structurally, microburst outflows were found to resemble the well-studied laboratory wall jet for both radial and vertical profiles of horizontal velocity, extending radially outward from the downdraft center to the outflow velocity maxima. Beyond this distance horizontal outflow velocities decreased more rapidly, and the presence of horizontal rotors complicated the airflow in the microburst. The effects of ambient winds were also in agreement with effects expected from wall-jet studies.

Temporal evolution of outflows showed an increase in ΔV to a maximum value followed either directly by decay or with an intervening period of near constant ΔV or pulsations. Outflows grew in size until maximum ΔV. After maximum ΔV, they either remained nearly constant in size until they dissipated or continued to grow until they became larger-scale outflows.

The results of this study confirm the previous work of Wilson et al. (1984) which concluded that outflow asymmetries create a significant problem for the estimation of shear along a particular path.

Acknowledgments. The author gratefully acknowledges K. Elmore, C. Kessinger, and R. Roberts for use of analyzed multiple-Doppler wind fields, and R. Roberts, W. C. Lee, and J. Wilson for use of edited radar data for my own synthesis and discussion. The efforts of L. Reum, P. Kucera, and A. Pignotti who assisted with the statistics are greatly appreciated. Special thanks are due K. Goodrich for introducing me to the literature on wall jets and for many helpful discussions, and to J. Wilson for his advice and support throughout the course of this study. I also wish to thank K. Elmore and Brad Ratcliffe for their assistance with figure composition, and S. Campbell, R. Carbone, K. Goodrich, C. Kessinger, J. McCarthy, R. Roberts, and J. Wilson for their comments on this work and manuscript, and J. Walters for editorial review. The manuscript was typed by D. Davis and M. Miller. Special thanks are due to NCAR Scientific Support Services for their outstanding performance in preparing the figures.

This work was funded partially by NCAR, the National Science Foundation, and the FAA (through Interagency Agreement DTFA01-82-Y-10513).

REFERENCES

Anderson, J. R., 1988: Numerical simulation of thunderstorm microburst outflows. Submitted to *Mon. Wea. Rev.*

Bedard, A. J., Jr., and T. J. LeFebvre, 1986: Surface measurements of gust fronts and microbursts during the JAWS project: Statistical results and implications for wind shear detection, prediction, and modeling. NOAA Tech. Memo. ERL WPL-135, 112 pp.

Bradshaw, P., and E. M. Love, 1959: The normal impingement of a circular air jet on a flat surface. ARC R and M 3205, September 1959.

——, and M. T. Gee, 1960: Turbulent wall jets with and without an external stream. ARC R and M 3252, June 1960.

Brock, F. V., and P. K. Govind, 1977: Portable Automated Mesonet in operation. *J. Appl. Met.*, **16**, 299–310.

Byers, H. R., and R. R. Braham, Jr., 1949: *The thunderstorm.* U.S. Government Printing Office, Washington, DC 287 pp.

Eilts, M. D., and R. J. Doviak, 1987: Oklahoma downbursts and their asymmetry. *J. Climate Appl. Meteor.*, **26**, 69–78.

Elmore, K. L., J. McCarthy, W. Frost and H. P. Chang, 1986: A high resolution spatial and temporal multiple Doppler analysis of a microburst and its application to aircraft flight simulation. *J. Climate Appl. Meteor.*, **25**, 1398–1425.

Federal Aviation Administration, 1987: Integrated FAA Wind Shear Program Plan. Development and Logistics, Aviation Standards, and Air Traffic, DOT/FAA, Washington, DC 20591. (Available through NTIS, Springfield, VA 22161.)

Frush, C., 1981: Doppler signal processing using IF limiting. *Preprints, 20th Conf. on Radar Meteorology,* Boston, Amer. Meteor. Soc., 332–337.

Fujita, T. T., 1979: Objectives, operations, and results of project NIMROD. *Preprints, 11th Conf. on Severe Local Storms,* Kansas City, Amer. Meteor. Soc., 259–266.

——, 1981: Tornadoes and downbursts in the context of generalized planetary scales. *J. Atmos. Sci.*, **38**, 1511–1534.

——, 1985: The downburst: Microburst and macroburst. Satellite and Mesometeorology Research Project, Research Pap. No. 210, University of Chicago, 122 pp.

——, 1986: DFW microburst on August 2, 1985. Satellite and Mesometeorology Research Project, Research Pap. No. 217, University of Chicago, 150 pp.

——, and H. R. Byers, 1977: Spearhead echo and downburst in the crash of an airliner. *Mon. Wea. Rev.*, **105**, 129–146.

——, and F. Caracena, 1977: An analysis of three weather-related aircraft accidents. *Bull. Amer. Meteor. Soc.*, **58**, 1164–1181.

——, and R. M. Wakimoto, 1981: Five scales of airflow associated with a series of downbursts on 16 July 1980. *Mon. Wea. Rev.*, **109**, 1438–1456.

——, and ——, 1983: Microbursts in JAWS depicted by Doppler radars, PAM, and aerial photographs. *Preprints, 21st Radar Conf.,* Edmonton. Amer. Meteor. Soc., 638–645.

Glauert, M. B., 1956: The wall jet. *J. Fluid Mech.*, **1**, 625–656.

Hjelmfelt, M. R., 1987: The microbursts of 22 June 1982 in JAWS. *J. Atmos. Sci.*, **44**, 1646–1665.

——, and R. D. Roberts, 1985: Microburst lines. *Preprints, 14th Conf. Severe Local Storms,* Indianapolis, Amer. Meteor. Soc., 297–300.

——, —— and H. D. Orville, 1986: Observational and numerical study of a microburst line-producing storm. *Preprints, 23rd Conf. on Radar Meteorology,* Snowmass. Amer. Meteor. Soc., J77–J80.

Kacker, S. C., and Whitelaw, J. H., 1968: Some properties of the two-dimensional turbulent wall jet in a moving stream. *J. Appl. Mech.,* Trans. ASME, Series E, **35**, 641–651.

Kessinger, C., M. Hjelmfelt and J. Wilson, 1983: Low-level microburst wind structure using Doppler radar and PAM data. *Preprints, 21st Conf. Radar Meteor.,* Edmonton, Amer. Meteor. Soc., 609–615.

——, P. S. Ray and C. E. Hane, 1987: The 19 May 1977 Oklahoma squall line. Part I: A multiple Doppler analysis of convective and stratiform structure. *J. Atmos. Sci.*, **44**, 2840–2864.

——, D. B. Parsons and J. W. Wilson, 1988: Observations of a storm containing misocyclones, downbursts, and horizontal rotor circulations. Accepted by *Mon. Wea. Rev.*

Knupp, K. R., 1987: Downdrafts within High Plains cumulonimbi. Part I: General kinematic structure. *J. Atmos. Sci.*, **44**, 987–1008.

Kropfli, R. A., 1986: A microburst observed by high resolution dual-Doppler radar. *Preprints, 23rd Conf. on Radar Meteorology,* Snowmass. Amer. Meteor. Soc., J109–J112.

Krueger, S. K., and R. M. Wakimoto, 1985: Numerical simulation of dry microbursts. *Preprints, 14th Conf. Severe Local Storms,* Indianapolis, Amer. Meteor. Soc., 163–166.

——, —— and S. J. Lord, 1986: Role of ice phase microphysics in dry microburst simulations. *Preprints, 23rd Conf. on Radar Meteorology,* Snowmass, Amer. Meteor. Soc., J73–J76.

McCarthy, J., and J. Wilson, 1985: The Classify, Locate, and Avoid Wind Shear (CLAWS) Project at Denver's Stapleton International Airport: Operational testing of terminal weather hazard warnings with an emphasis on microburst wind shear. *Preprints, 2nd Int'l. Conf. Aviation Weather Systems,* Montreal, Amer. Meteor. Soc., 247–256.

——, —— and T. T. Fujita, 1982: The Joint Airport Weather Studies Project. *Bull. Amer. Meteor. Soc.*, **63**, 15–22.

Mahoney, W. P., III, and A. R. Rodi, 1987: Aircraft measurements on microburst development from hydrometeor evaporation. *J. Atmos. Sci.*, **44**, 3037–3051.

Merritt, M. W., 1987: Automated detection of microburst windshear for terminal Doppler weather radar. *Preprints, Digital Image Processing and Visual Communications Technology in Meteorology,* Cambridge, Oct., SPIE, Bellingham.

Mohr, C. G., L. J. Miller, R. L. Vaughan and H. W. Frank, 1986: The merger of mesoscale data sets into a common Cartesian format for efficient and systematic analyses. *J. Atmos. Ocean. Tech.*, **3**, 143–161.

Mueller, C. K., and P. H. Hildebrand, 1963: The structure of a microburst: As observed by ground-based and airborne Doppler radar. *Preprints, 21st Radar Meteor. Conf.,* Edmonton, Amer. Meteor. Soc., 602–608.

Nathanson, F. E., 1969: *Radar design principles.* McGraw Hill, 596 pp.

National Research Council, 1983: Low altitude wind shear and its hazard to aviation. National Academy Press, 161 pp.

Oye, R., and R. Carbone, 1981: Interactive Doppler editing software. Preprints, *20th Radar Meteor. Conf.*, Boston, Amer. Meteor. Soc., 683–689.

Poreh, M., and J. E. Cermak, 1959: Flow characteristics of a circular submerged jet impinging normally on a smooth boundary. *Proceedings of the Sixth Midwest Conference on Fluid Mechanics,* Austin, Texas. University of Texas, 198–212.

——, Y. G. Tsuei and J. E. Cermak, 1967: Investigation of a turbulent radial wall jet. *J. Appl. Mech.*, Trans. ASME, Series E, **34,** 457–463.

Proctor, F. H., 1985: Numerical simulation of precipitation induced downbursts. *Preprints, 2nd Int. Conf. Aviation Weather Systems,* Montreal, Amer. Meteor. Soc., 257–264.

——, 1988: Numerical simulations of an isolated microburst, Part I Dynamics and Structure. Accepted for publication in *J. Atmos. Sci.*

Rinehart, R. E., J. T. DiStephano and M. M. Wolfson, 1987: Preliminary Memphis FAA/Lincoln Laboratory operational weather studies results. DOT/FAA/PM-86-40, 198 pp.

Roberts, R. D., and J. W. Wilson, 1984: Precipitation and kinematic structure of microburst producing storms. *Preprints, 22nd Radar Meteor. Conf.*, Zurich, Amer. Meteor. Soc., 71–76.

——, and ——, 1986: Nowcasting microburst events using single Doppler radar data. *Preprints, 23rd Radar Meteor. Conf.,* Snowmass. Amer. Meteor. Soc., 14–17.

Sadeh, W. Z., and S. K. Mukherji, 1974: A wall jet in a shear stream. *Proceedings, 11th Annual Meeting Society of Engineering Science,* Duke University, Durham, N.C., 136–137.

Srivastava, R. C., 1985: A simple model of evaporatively driven downdraft: Application to microburst downdraft. *J. Atmos. Sci.,* **42,** 1005–1023.

——, 1987: A model of intense downdrafts driven by the melting and evaporation of precipitation. *J. Atmos. Sci.*, **44,** 1752–1773.

Stevenson, L., 1985: The Stapleton microburst advisory service experiment (an operational viewpoint). DOT Transportation Systems Report, DOT-TSC-FAA-85-8.

Waranauskas, B. R., 1985: The rotor microburst: A new explanation for burst swath damage. *Preprints, 14th Conf. on Severe Local Storms.* Indianapolis. Amer. Meteor. Soc., 260–263.

Wilson, J. W., and W. E. Schreiber, 1986: Initiation of convective storms by radar-observed boundary layer convergent lines. *Mon. Wea. Rev.*, **114,** 2516–2536.

——, R. D. Roberts, C. Kessinger and J. McCarthy, 1984: Microburst wind structure and evaluation of Doppler radar for airport wind shear detection. *J. Climate Appl. Meteor.*, **23,** 898–915.